Modelling Bisulfide Transport through the Engineered Barrier System under Repository Conditions: Coupling Unsaturated Flow and Refining Boundary Conditions

NWMO-TR-2022-06 March 2022

Md Abdullah Asad[1]

Tarek Rashwan[1]

Ian Molnar[2]

Magdalena Krol[1]

[1]York University, Canada
[2]University of Edinburgh, United Kingdom

nwmo
NUCLEAR WASTE MANAGEMENT ORGANIZATION
SOCIÉTÉ DE GESTION DES DÉCHETS NUCLÉAIRES

Nuclear Waste Management Organization
22 St. Clair Avenue East, 6th Floor
Toronto, Ontario
M4T 2S3
Canada

Tel: 416-934-9814
Web: www.nwmo.ca

Modelling Bisulfide Transport through the Engineered Barrier System under Repository Conditions: Coupling Unsaturated Flow and Refining Boundary Conditions

NWMO-TR-2022-06

March 2022

Md Abdullah Asad[1]
Tarek Rashwan[1]
Ian Molnar[2]
Magdalena Krol[1]

[1]Civil Engineering Department
Lassonde School of Engineering
York University, Canada

[2]School of Geosciences-University of Edinburgh, Edinburgh, Scotland

Document History

Title:	Modelling Bisulfide Transport through the Engineered Barrier System under Repository Conditions: Coupling Unsaturated Flow and Refining Boundary Conditions		
Report Number:	NWMO-TR-2022-06		
Revision:	R000	Date:	March 2022
Authored by:	Md Abdullah Asad[1], Tarek Rashwan[1], Ian Molnar[2], and Magdalena Krol[1]		
Company:	[1]York University, Canada [2]School of Geosciences-University of Edinburgh, Edinburgh, Scotland		
Nuclear Waste Management Organization			
Reviewed by:	Mehran Behazin Peter Keech		
Accepted by:	Chris Boyle		

ABSTRACT

Title: **Modelling Bisulfide Transport through the Engineered Barrier System under Repository Conditions: Coupling Unsaturated Flow and Refining Boundary Conditions**

Report No.: **NWMO-TR-2022-06**

Authors: Md Abdullah Asad[1], Tarek Rashwan[1], Ian Molnar[2], and Magdalena Krol[1]

Company: [1]York University, Canada

[2]School of Geosciences-University of Edinburgh, Edinburgh, Scotland

Date: March 2022

The Canadian Nuclear Waste Management Organization (NWMO) has proposed a deep geological repository (DGR) as a long-term solution for management of Canada's used nuclear fuel. The DGR is designed to isolate radionuclides via an engineered barrier system (EBS), constructed at least 500 m deep into low permeability host rock (either crystalline or sedimentary). The EBS consists of used fuel containers (UFCs) made of carbon steel, coated with 3 mm of copper to form a corrosion resistant barrier surrounded by highly compacted bentonite (HCB) clay. Although the copper coating is thermodynamically stable in oxygen-free environments, it is susceptible to microbiologically influenced corrosion (MIC) during anoxic conditions. Depending on site-specific conditions (e.g., host rock type, groundwater chemistry, microbial growth conditions), bisulfide or other sulfide-containing species, produced by sulfate-reducing bacteria near the host rock-bentonite interface could transport slowly through the HCB to the UFC surface and corrode the copper coating. This transport is affected by the transient conditions in the DGR, such as saturation, temperature, microbial, and geochemical conditions. These conditions are all interconnected and require a robust numerical model to best understand their impacts on bisulfide transport mechanisms. Therefore, this report describes a numerical model that can capture these interconnected processes and provide a flexible tool to aid in assessing the DGR performance as site-specific information becomes available.

This report outlines the long-term conditions anticipated in the DGR, conceptual models of the processes affecting MIC, and results of a newly developed, coupled two-dimensional (2-D) and three-dimensional (3-D) Thermal-Hydraulic-Chemical (Diffusion) model (THC model). The THC model simulates bisulfide transport through the DGR in variably saturated and non-isothermal conditions. Moreover, the specific implementation, verification, and validation procedures have been documented and are presented herein.

The repository was approximated as a 2-D and 3-D system, assuming the host rock was either crystalline or sedimentary and all parameters were obtained from NWMO case studies and other studies. Several assumptions were made to develop the model. Advective mass transport and convective heat transport were not considered due to low bentonite permeability. In addition, no sorption, geochemical reactions, microbial reactions, vapour transport, and bentonite swelling were considered. A range of verification procedures were conducted to develop confidence in the model. A mesh convergence study was performed to ensure the model was properly discretized, and a sensitivity study on various boundary conditions was performed to ensure correct conditions were implemented. It was found that a domain depth of 10,000 m accurately predicted the temperature profile. In addition, constant pressure head conditions were used at the model flow boundaries to realistically describe the saturation conditions and avoid anomalous low pressure zones that developed with no-flow boundaries. Around the UFC, a boundary heat source was chosen to model the heat generated by the used nuclear fuel, as a domain heat source overpredicted the UFC temperature due to geometry and modelling inputs. Lastly, the host rock was assumed to be fully saturated while the HCB was initially at 67% saturation while a constant, 1 ppm bisulfide concentration boundary condition was conservatively assumed to be at the rock-bentonite interface. The 2-D THC model was compared with previous models

developed by Briggs and Krol (2018). A 3-D THC model was also developed and compared with the 2-D THC model. Lastly, the robustness of the numerical approximation used in the model was confirmed through good agreement between numerical and theoretical solutions.

Overall, the THC model predicted 20 years and 160 years for full saturation in the crystalline and sedimentary DGR, respectively. These saturation times are generally briefer, yet still comparable to the results from other HCB saturation studies assuming similar host rock conditions, i.e., 10's-100's of years (e.g., DECOVALEX III project results). Typically, increasing rock permeability would decrease bentonite saturation time. However, in the crystalline domain, the saturation times are insensitive to rock permeability since the rock permeability is higher than the bentonite permeability, making the bentonite the governing layer. As bisulfide transport is diffusion dominated, and no gaseous transport is assumed, bisulfide transport starts as the EBS becomes saturated. The maximum bisulfide flux occurs at the hemi-spherical end caps of the UFC due to UFC and EBS geometry. Presuming the incoming bisulfide reacts with the copper coating with 100% efficiency and MIC occurs instantaneously at the UFC surface, the total maximum MIC depths are 0.645 mm and 0.517 mm in million years in the sedimentary and crystalline DGR, respectively. In addition, a model comparison (THC versus previous models developed by Briggs and Krol (2018)) reveals that the MIC is driven by changes in saturation and UFC temperature that impact bisulfide diffusion rates, which only occurs during the initial life span of the DGR (i.e., before 200,000 - 400,000 years). After this time, MIC occurs due to diffusion only in a saturated system under isothermal conditions. The 3-D THC model, set in the crystalline DGR, results in a total MIC depth of 0.671 mm. This difference occurs due to 3-D geometry, which captures MIC rates in the third dimension that are not included in the 2-D model. However, the characteristic UFC temperature and degree of saturation are very similar between the 2-D and 3-D models.

These observations in the boundary condition effects, EBS temperature, saturation time, and bisulfide transport revealed by the model are discussed in detail in this report. These observations provide deeper insight into the anticipated MIC in the DGR, thereby providing valuable information for assessing the DGR performance.

TABLE OF CONTENTS

LIST OF FIGURES

LIST OF TABLES

1 INTRODUCTION

In response to the need for a long-term solution for disposal of Canada's used nuclear fuel, the Canadian Nuclear Waste Management Organization (NWMO) developed the "Adaptative Phase Management (APM)" for Canada's deep geological repository (DGR). This plan is a combination of both technical mechanisms and a management system, which aims to isolate used nuclear fuel in a DGR located within crystalline or sedimentary rock, about 500 m deep below the ground surface. The NWMO expects to select a DGR construction site by 2023 and apply for a license by 2028 (NWMO 2018). Under the APM, the NWMO is working with Canadian universities, scientists, and other countries' nuclear safety organizations to build confidence in the DGR design by performing a robust performance assessment with state-of-the-art predictive tools.

The NWMO's DGR design includes an engineered barrier system (EBS) within placement rooms constructed in a low permeability host rock, which acts as a natural barrier. The EBS consists of used fuel containers (UFCs) made of carbon steel and coated with 3 mm of copper, which serves as a corrosion resistant barrier. The UFCs are designed to hold 48 bundles of CANDU fuel (Canada deuterium uranium), and are surrounded by highly compacted bentonite (HCB) blocks (referred to as the "buffer box") (Hall et al. 2021) (Figure 1). The HCB spacer blocks separate the buffer boxes. Blocks are fabricated by compressing Wyoming bentonite with a moisture content of around 20% in a cold isostatic press (NWMO 2019). Blocks are subsequently shaped using slow rotation machining tools. The specification for dry density of HCB is ≥ 1700 kg m^{-3}. Gapfill material (GFM) will be used to fill the void spaces between the HCB and the DGR rock walls. GFM uses the same bentonite as the HCB. GFM is fabricated by roll compacting with a moisture content of <5% milling, sieving, and blending to produce a well-graded granular material with a maximum size of 8 mm (NWMO 2019). The well-graded particle size distribution helps provide a good flowability to meet a specification for dry density of ≥ 1410 kg m^{-3}.

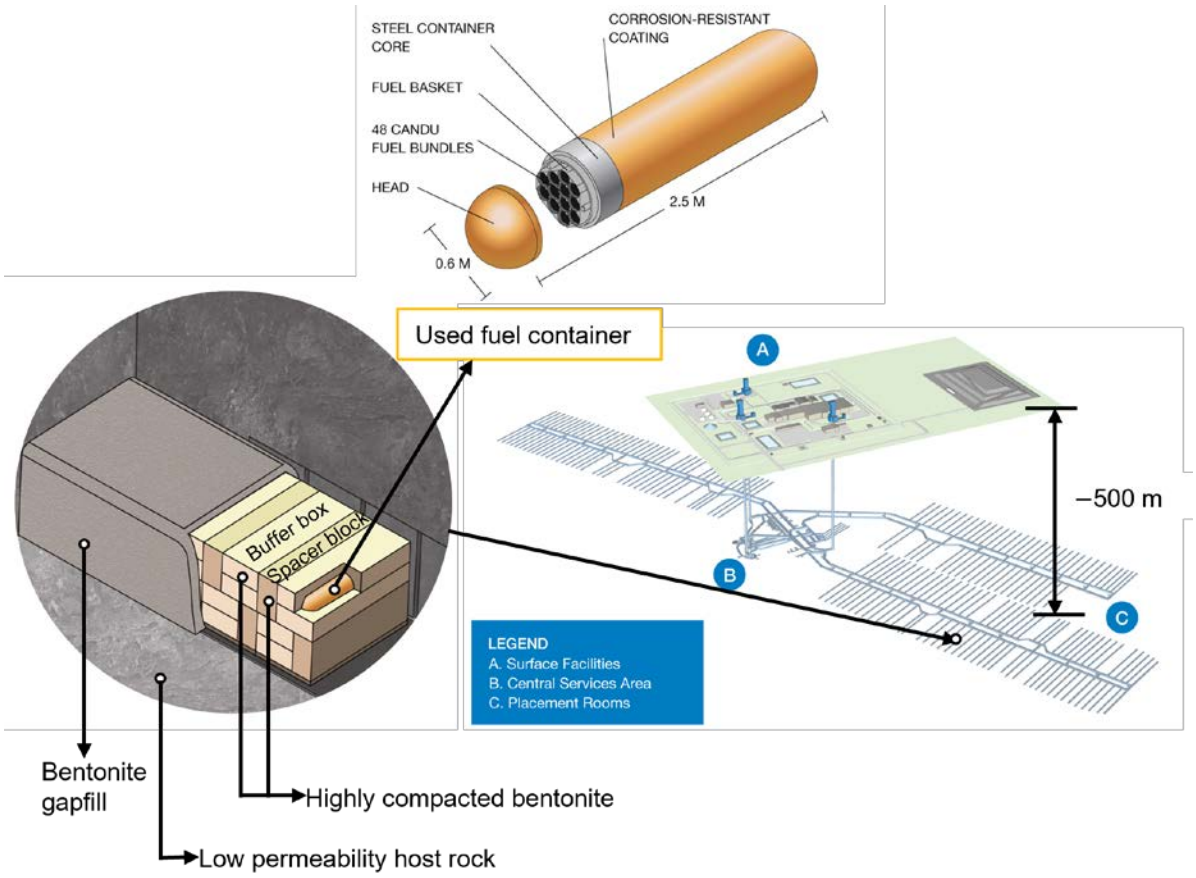

Figure 1: Multiple Barrier System in Canadian DGR (Adapted from Hall et al. (2021))

The objective of this report is to showcase an extension of a numerical model originally developed by Briggs and Krol (2018), as well as a verification and validation study of the model to aid in the assessment of the DGR under a range of conditions. This model couples DGR temperature evolution, bentonite saturation, and bisulfide transport to simulate UFC corrosion driven by bisulfide. Bisulfide is anticipated to be generated at the rock-bentonite interface by sulfate-reducing bacteria, diffusive through the bentonite and reach the UFC where it can corrode the copper (i.e., microbiologically-influenced corrosion (MIC)). This report outlines long term evolution of DGR conditions and the conceptual model framework of the coupled DGR processes. Moreover, verification and validation studies are presented including mesh convergence tests and comparisons with similar studies, respectively.

2 BACKGROUND

As part of the EBS, HCB was chosen as it possesses good sealing properties against groundwater infiltration (i.e., low intrinsic permeability and self-sealing due to swelling), can retard transport of radionuclides in the event of a UFC breach, and suppress microorganism activity near the UFC (Stroes-Gascoyne et al. 2010). In addition, the HCB can also limit the flux of corrosive species from the surrounding subsurface. The DGR near-field environment, where the HCB is placed, will evolve from an initially warm and oxic environment to a cool and anoxic condition in a span of a million years (King et al 2017) although the depletion of oxygen is anticipated to occur within a period of a few months (Giroud et al. 2018) to a few years (Johansson et al. 2020). In addition, the bentonite will saturate as water infiltrates from the host rock. Under saturated-anoxic conditions, bisulfide may be produced through microbial processes at the rock-bentonite interface and could transport through the HCB to the UFC surface where it could corrode the UFC's copper coating. The long-term prediction of this corrosion is necessary to aid in the performance assessment of the barrier system design and ensure adequate corrosion allowance. This prediction requires conceptual understanding of the time-dependent evolution of the DGR environment (Figure 2), which includes changes in different physical and chemical processes (King et al 2017).

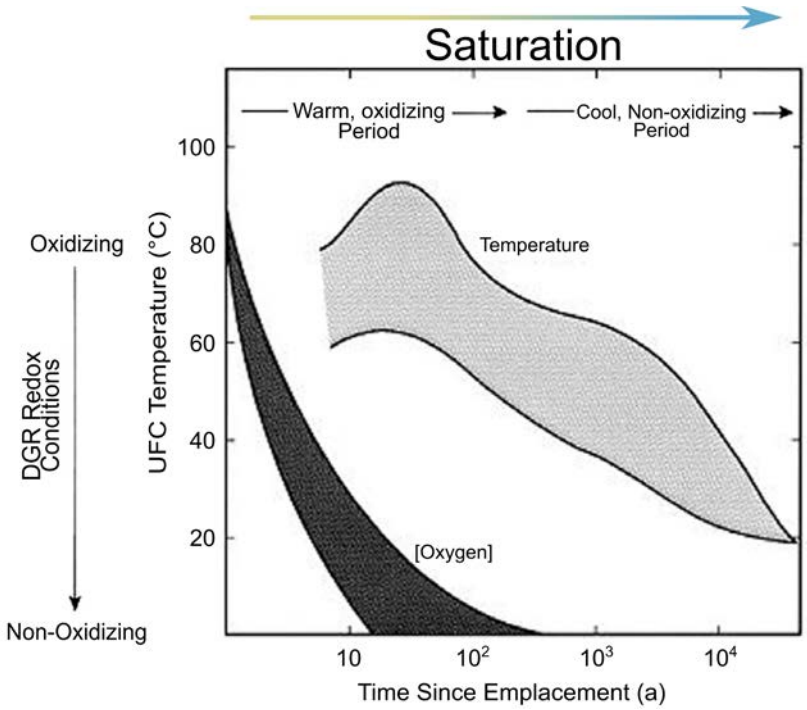

Figure 2: Approximated DGR Environmental Conditions (Adapted from (King et al. 2008) with permission of Elsevier)

2.1 TEMPERATURE EVOLUTION

According to King et al. (2008) and Guo (2016), DGR temperature will gradually increase due to the heat produced from the used fuel, reaching a peak temperature of above 80 ˚C after 10 years and then decrease gradually to approximately 20 ˚C over 10,000 years (Figure 2). Understanding this temperature evolution is important as thermal gradients in the bentonite buffer may dry the bentonite initially and stop aqueous UFC corrosion (King et al. 2017). Moreover, it may impact the UFC corrosion behaviour as reaction rates and solubility of minerals (i.e., bentonite clay minerals) vary with temperature (King et al. 2017). Temperature may also affect bentonite saturation and bisulfide aqueous diffusion through the bentonite as solute diffusion rates also vary with temperature (Einstein 1905; King et al. 2017).

2.2 EVOLUTION OF BENTONITE SATURATION AND OXIC CONDITIONS

The bentonite is expected to gradually saturate with time, increasing from initial saturation to fully saturated conditions (Figure 2). The saturation time will vary with the host rock type (King et al 2017), temperature gradient (Villar et al. 2012), bentonite density and permeability, and initial saturation conditions. The current assumption is that the DGR will fully saturate within 50 years for crystalline rock and 5,000 years in sedimentary rock (King et al 2017).

Initial saturation of the emplaced HCB in the Canadian DGR design has evolved from 65% to 89%. According to the current Canadian DGR design, the emplaced HCB will have an initial saturation of 89% and the GFM will have an initial saturation of 9% (Gobien et al. 2016; King et al. 2017; Dixon 2019; Dixon et al. 2018). The heat evolved from the used fuel will dry the bentonite, and subsequent water infiltration from the host rock will saturate the bentonite once the temperature decreases (King et al. 2017). As the DGR host rock is expected to have low permeability, capillary dominated water flow will govern the saturation and bentonite swelling processes. The saturation rate may affect the rate of species transport through the bentonite to the UFC surface (King et al. 2017), as aqueous dissolved species will only transport through partially and fully saturated pores and no aqueous transport will occur in unsaturated clay (unsaturated being defined as no water-connected pores present). In addition, the saturation process may affect the temperature distribution in the DGR (King et al. 2017). Overall, the DGR will undergo a range of saturation conditions (i.e., unsaturated, partially saturated, and fully saturated) throughout its lifetime (Figure 2).

The initial DGR redox condition will be oxic due to entrapped air leftover from DGR construction and operation. The amount of initial oxygen can be estimated using the buffer properties (porosity, degree of saturation, solubility in water), and ideal gas law (Hall et al. 2018). Typically, the oxygen content is assumed to be 1 to 10 mol per m^2 of the UFC surface for oxic copper corrosion (King et al. 2017). However, this value would be lower (Hall et al. 2018), as oxygen may be consumed by other processes, for example, oxidation of minerals in the host rock and bentonite, and aerobic microbial activity (King et al. 2017). The speed of these processes will govern the oxic period length, which is important as it will affect the oxic corrosion processes such as uniform copper corrosion (UC) and stress corrosion cracking (SCC); although, copper is not generally susceptible to SCC (Scully et al. 2016; King et al. 2017). The prediction for the duration of the oxic period is dependent on the processes that occur in the repository. It has been conservatively estimated to be less than a century by King et al (2008).However, recent field studies at the Mont Terri Underground Laboratory suggest a shorter oxic period of less than 1.5 years (Müller et al. 2017) Even more recent large-scale *in situ* experiments indicate that the O_2 is fully consumed within a period of a few months (Giroud et al 2018) to a few years (Johansson et al. 2019). All are very brief when compared to the anoxic period length, which will persist throughout the rest of the DGR lifespan of hundreds of thousands or millions of years. Accordingly, the anoxic period will govern many long-term processes in the DGR (King et al. 2017). Table 1 shows the evolution of the DGR conditions under three different phases in the DGR (as discussed above). These phases are distinct in terms of their bentonite saturation, temperature, bentonite swelling, and redox conditions.

Table 1: Evolution of DGR Conditions with Time (Adapted from (King 2005))

Property	Initial Phase	Transition Phase	Final Phase
Temperature	Temperature increases	Temperature decreases	Temperature reaches background levels
Saturation	Redistribution of initial moisture content	Gradual saturation of bentonite	Complete saturation of bentonite
Thermal Conduction	Poor thermal conduction	Thermal conduction improves	Good thermal conduction
Bentonite Swelling	No swelling of bentonite	Bentonite swelling starts	Bentonite swelling complete
Redox condition	Oxic	Oxic/Anoxic	Anoxic

2.3 MICROBIOLOGICALLY INFLUENCED CORROSION

After the consumption of the initially trapped oxygen anoxic conditions will govern in the subsurface. Anoxic UFC corrosion may occur through microbiologically influenced corrosion (MIC) if bisulfides (HS^-) are present or produced in the DGR. Bisulfide may be produced at the rock-bentonite interface due to sulfate reduction by sulfate-reducing bacteria (SRB). If bisulfide transports through the bentonite to the UFC, it may corrode the copper barrier via the simplified reaction below (Cloet et al. 2017):

$$2Cu_{(s)}+HS^-_{(aq)}+H^+_{(aq)}\leftrightarrow Cu_2S_{(s)}+H_{2(g)} \quad (1)$$

Equation 1 describes the anoxic corrosion of copper in the presence of aqueous bisulfide which is likely to be the largest contributor to long-term copper corrosion in the DGR (Hall et al, 2021). Although bentonite in the Canadian DGR will prevent microbial activity near the container due to its high density, which lowers the water activity (King 2008, Pedersen 2010), SRB may be active at or beyond the bentonite-rock interface and drive HS^- production (King et al. 2002; King 2009; Stroes-Gascoyne et al. 2010; Standish et al. 2016; Cloet et al. 2017). Due to the persistence of this condition for a very long time period, previous studies estimated MIC as the highest UFC corrosion contributor compared to other types of corrosion (Figure 3).

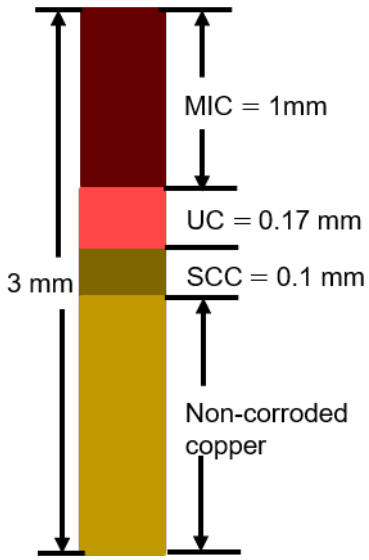

Figure 3: Estimated Copper Corrosion Depth (Modified from (Keech et al. 2021))

2.4 CONCEPTUAL MODEL OF COUPLED PROCESSES IN CANADIAN DGR

Figure 4 represents the key phenomena expected in a DGR. Heating from the UFC establishes a thermal gradient across the EBS (high temperature near the UFC and low temperature near the host rock) with saturation occurring in the opposite direction – from host rock to UFC (Sena et al. 2010). The saturation process under this thermal gradient can affect diffusion-dominated transport through the bentonite as diffusion is assumed to only occur in the water phase therefore it is limited in partially saturated systems (Martín et al. 2000). In addition, the interlinking between saturation and heating could complicate the diffusive transport of corrosive species. Geochemical reactions (e.g., precipitation, dissolution) can also occur within the bentonite, causing changes in the bentonite porewater chemistry and bentonite pore structure (Villar et al. 2012) with implications for bisulfide flux through the bentonite (Wersin et al. 2014).

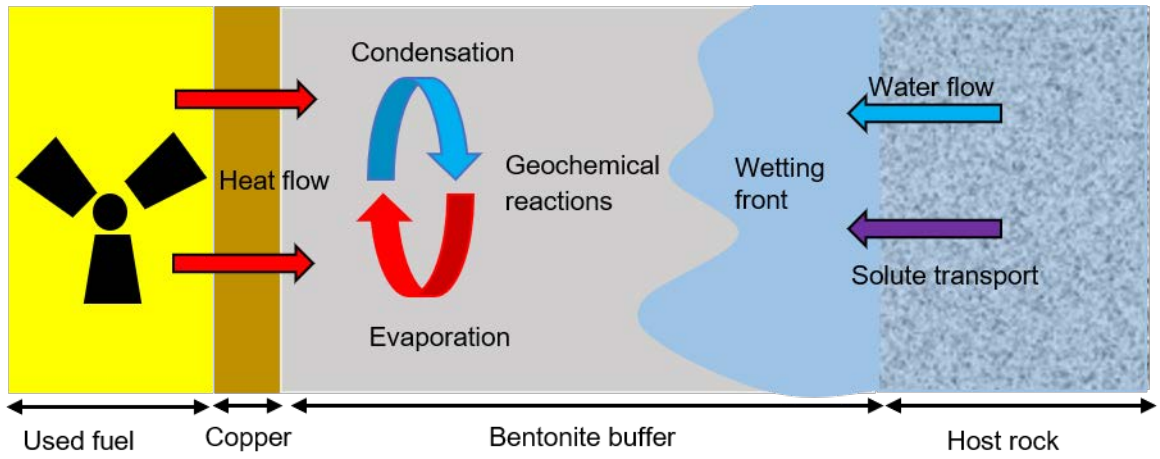

Figure 4: Key DGR Transport Processes (Adapted from Sena et al. (2010))

Figure 5 shows how the governing processes (identified in Figure 4) are coupled in the Canadian DGR environment. As bentonite saturates, it will swell, and its permeability and water activity will be reduced. Due to the heat produced from UFCs, some groundwater will evaporate and become water vapour. This water vapour will either transport through the bentonite pores or condense back to the liquid phase. Sulfate present in the rock or groundwater may be reduced to bisulfide through SRB, but its flux through the EBS will depend upon the geochemical reactions within the bentonite, the bentonite and water properties, and bentonite degree of saturation. More specifically, bisulfide diffusion through the bentonite will depend upon the bentonite properties (e.g., density, porosity, tortuosity, sorption, saturation) and water properties (e.g., temperature, salinity). The bisulfide that reaches the UFC surface, despite the low permeability and high adsorptive capacity of bentonite, can corrode the copper surrounding the UFC.

While the ultimate goal of the model is to include all the processes discussed above, the current study considers the phenomena highlighted in red in Figure 5, including bisulfide transport, water saturation, and heat generation. This conceptual model in Figure 5 informs the experimental and numerical studies related to DGR safety analysis and provides valuable information about the importance of certain phenomena and interactions. At the same time, as the information through models and experiments become available, some of these interactions may be found to be insignificant, which may necessitate revisiting the conceptual model.

The goal of the Thermal-Hydraulic-Chemical (Diffusion) model (referred to as the “THC model”) is to explore the impact of the highly coupled processes illustrated in Figures 4 and 5 on DGR performance and answer key questions including: how long will it take to fully saturate the

bentonite, how do various parameters affect bisulfide transport, what is the distribution of bisulfide flux over the UFC surface, and what is the estimated MIC depth?

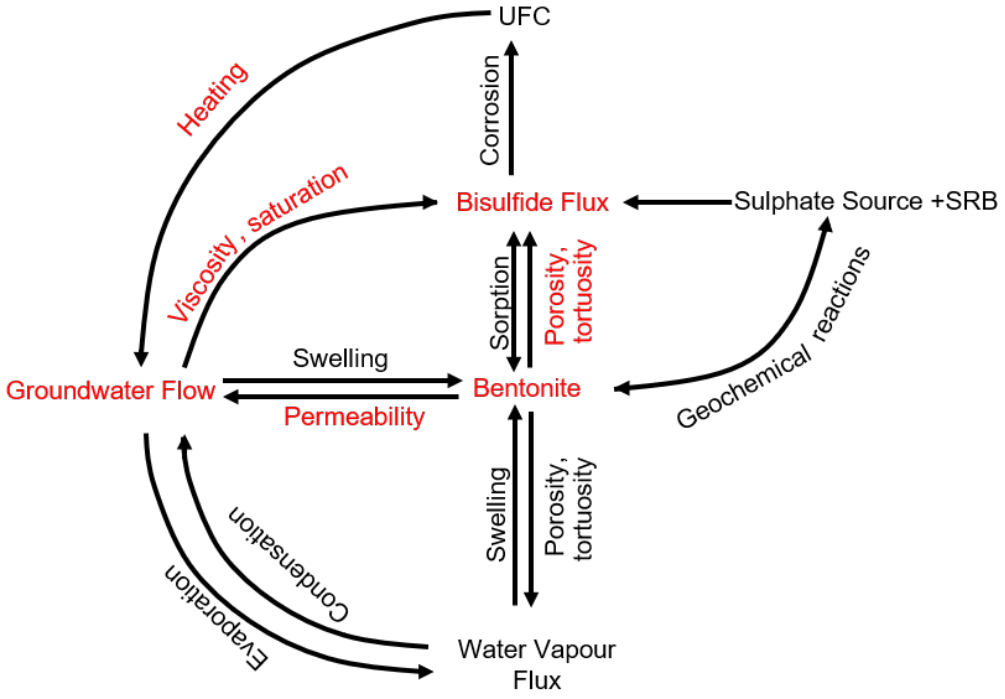

Figure 5: Coupled DGR Processes Governing MIC and Saturation Of DGR; Red Font Indicates Processes Modelled in This Study

3 MODEL APPORACH AND METHODOLOGY

This section discusses the development, mesh convergence, and validation of the newly coupled 2-D and 3-D Thermal-Hydraulic-Chemical (Diffusion) model (referred to as the "THC model"). This modelling work directly builds upon the work from Briggs and Krol (2018) who developed DGR models using COMSOL Multiphysics, a commercial finite element software package. They explored the effects of saturation and temperature separately on bisulfide transport and MIC. The THC model presented herein extends their work to explore the combined effect of temperature and saturation on bisulfide transport using a non-isothermal and variably saturated model as well as extending it to three dimensions. Like Briggs and Krol (2018), no sorption and geochemical reactions, vapour transport, and bentonite swelling were considered (see Figure 5 for modelled processes in current study).

The transport of aqueous dissolved compounds (bisulfide) is governed by diffusion due to the low permeability of bentonite (mass Peclet number of 2×10^{-4}) and is described by Fick's 2nd law (Fick 1855) as follows:

$$\varepsilon \frac{\partial C}{\partial t} + C C_m \frac{\partial H_p}{\partial t} = D_e \nabla^2 C \qquad (2)$$

Where ε is the porosity, C is the bisulfide aqueous concentration, C_m is the specific moisture capacity, and D_e is the effective bisulfide diffusion coefficient. The transient heat equation was used to model energy transfer, also dominated by thermal diffusion:

$$\rho_s c_p \frac{\partial T}{\partial t} = \nabla(k_{eff} \cdot \nabla T) + q(t) \qquad (3)$$

Where T is the temperature, k_{eff} is the effective thermal conductivity, c_p is the specific heat, ρ_s is the density, and q is the heat source. Richards' equation (Richards 1931) was used to model water infiltration into the DGR:

$$(C_m+S_eS_s)\frac{\partial H_p}{\partial t}+\nabla\cdot\left(-K\nabla\left(H_p+z\right)\right)=0 \tag{4}$$

Where S_e is the effective saturation of the bentonite, S_s is the storage coefficient, H_p is the pressure head, K is the soil or rock hydraulic conductivity, and z is the depth of the system. The constitutive relationships used within Richards' equation to model unsaturated flow followed the formulations from van Genuchten (1980):

$$S=\begin{cases} S_r+S_e(S_f-S_r) & H_p<0 \text{ m} \\ S_f & H_p\geq 0 \text{ m} \end{cases}$$

$$S_e=\begin{cases} \dfrac{1}{\left(1+\left|\alpha H_p\right|^n\right)^m} & H_p<0 \text{ m} \\ 1 & H_p\geq 0 \text{ m} \end{cases}$$

$$C_m=\begin{cases} \dfrac{\alpha m}{1-m}(\varepsilon S-\varepsilon S_r)S_e^{\frac{1}{m}}\left(1-S_e^{\frac{1}{m}}\right)^m & H_p<0 \text{ m} \\ 0 & H_p\geq 0 \text{ m} \end{cases}$$

$$k_r=\begin{cases} S_e^{0.5}\left(1-\left[1-S_e^{\frac{1}{m}}\right]^m\right)^2 & H_p<0 \text{ m} \\ 1 & H_p\geq 0 \text{ m} \end{cases} \tag{5}$$

Where S, S_f, and S_r are the saturation, full saturation, and residual saturation, respectively, k_r is the relative permeability, α, n, and m are constant properties inherent to the soil and are given in Table 2 (note that m=1- 1/n). Equations 2-4 are the governing equations in the THC model. The interactions between the governing equations are captured in temperature and saturation-dependent parameters. For example, k_{eff} and effective heat capacity, $\rho C_{P_{eff}}$, are functions of ε, S, while they are dependent on the heat capacity and thermal conductivity of water (k_w, C_{P_w}), bentonite (k_s, C_{P_s}), and air (k_a, C_{P_a}), as seen through equations 6 and 7.

$$\rho C_{P_{eff}}=\varepsilon\rho_w S C_{P_w}+(1-\varepsilon)\rho_s C_{P_s}+\varepsilon\rho_a(1-S)C_{P_a} \tag{6}$$

$$k_{eff}=\varepsilon k_w S+(1-\varepsilon)k_s+\varepsilon k_a(1-S) \tag{7}$$

The soil hydraulic conductivity is also a function of soil permeability, water density (ρ_w), and dynamic viscosity of water (μ) which are temperature dependent. The relationship between bisulfide diffusion coefficient in water, temperature, and viscosity of water was defined as follows (Einstein, 1905):

$$\frac{D_{T_1}}{D_{T_2}}=\frac{T_1}{T_2}\frac{\mu_{T_2}}{\mu_{T_1}} \tag{8}$$

Where D is the bisulfide diffusion coefficient in water, T_1 and T_2 are the respective temperatures and μ is the dynamic viscosity of water at the various temperatures.

Lastly, the effective bisulfide diffusion coefficient in bentonite is a function of bisulfide diffusion coefficient in water, saturation, diffusion accessible porosity (ε_e), and tortuosity (τ) following Shackelford and Moore (2013):

$$D_e = S\frac{\varepsilon_e}{\tau}D \tag{9}$$

$$\tau = \left(\frac{L_e}{L}\right)^2 \tag{10}$$

Where L and L_e are the straight-line and actual travel distances in the porous medium.

3.1 MODEL DEVELOPMENT

A single placement room and the surrounding host rock were approximated in 2-D and 3-D as shown in Figure 6. The EBS was placed 500 m below the ground surface and the model domain extended up to 9,500 m below this level (total domain of 10,000 m). The whole domain was symmetric about the two vertical axes (i.e., one half or quarter of the placement room and surrounding rock was simulated for 2-D and 3-D, respectively), which reduced the computational time. The parameters were obtained from NWMO case studies and other studies (Baumgartner 2006; SKB 2010; Guo 2016, 2018; Gobien et al. 2018; Sykes et al. 2011; Gobien et al. 2016; Dixon 2019; Dixon et al. 2018) while the UFC heating was estimated from Tait et al. (2000). The Richards' equation (Equation 4) simulated water movement into a partially saturated bentonite from a fully saturated host rock, the heat transfer equation (Equation 3) simulated conductive heat transfer, and Fick's law (Equation 2) simulated bisulfide diffusion through the bentonite due to a concentration gradient.

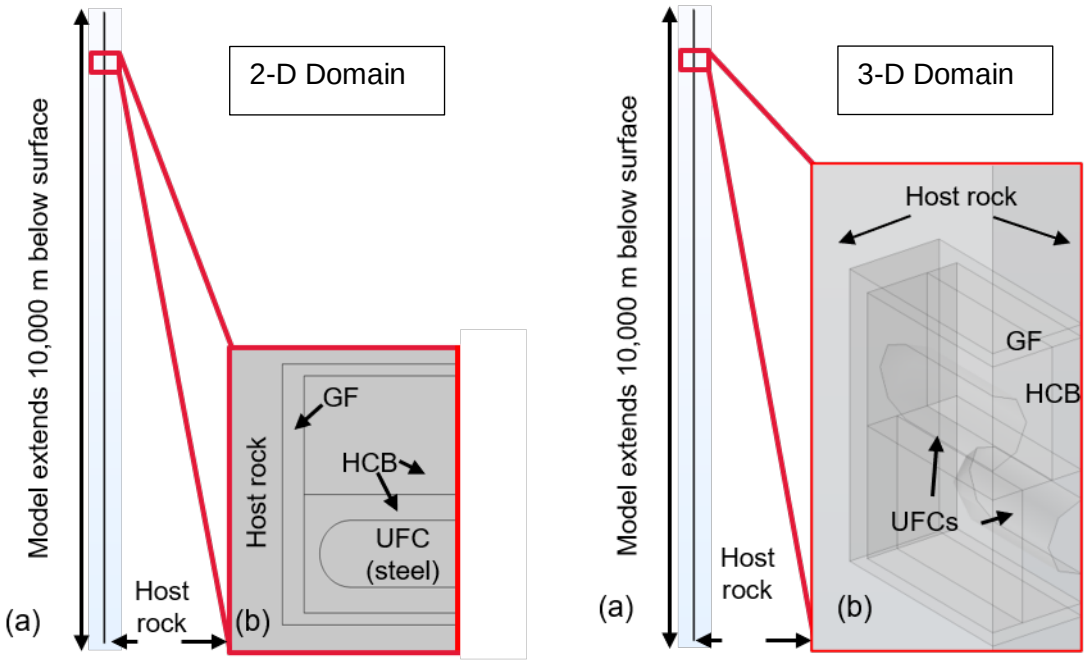

Figure 6: COMSOL Modelling Domain for: a) The Full 10,000 M Deep Domain and b) a 10 M Segment of a Single Placement Room, for Both 2-D And 3-D Domain. The Placement Room Contains One Used Fuel Container (UFC) in 2-D and Two UFCs in 3-D, Gap Fill (GFM), High Compacted Bentonite (HCB), and Host Rock.

The model boundary conditions, and mesh configurations are shown in Figure 7. This figure shows the 2-D domain; however, the third dimension has the same boundary conditions as the vertical axis shown. The pressure head boundary conditions were set at the top, sides and bottom of the domain to represent the system at hydrostatic equilibrium (Avis et al. 2012). The initial conditions assumed the host rock was assumed fully saturated, and the bentonite (HCB) and gap fill (GFM) were 67% saturated (6^{th} case study) (Figure 7a). An isothermal boundary was imposed on the ground surface (top boundary), at a temperature of 5 ˚C and 10 ˚C in the crystalline and sedimentary rock, respectively (Guo 2016, Guo 2018). The bottom boundary was also set as isothermal with temperatures of 125 ˚C and 113 ˚C in the crystalline and sedimentary rock, respectively, obtained from geothermal gradients of 0.012 ˚C/m and 0.0103 ˚C/m in the crystalline and sedimentary rock, respectively (Guo 2016, Guo 2018). The UFC heating was defined by a boundary heat source (i.e., along a line) and a domain heat source (i.e., over a volume) in the 2-D and 3-D models, respectively. An adiabatic symmetry boundary condition was applied on the outside vertical boundary which represents an infinite number of UFC heat sources (Figure 7b). The far field bisulfide concentration at the host rock-GFM (bentonite) interface was assumed to be 1 ppm (0.001 kg m^{-3}) and was implemented as a constant concentration boundary condition. This value was chosen as unity to help simplify conversion when site specific bisulfide concentrations for the Canadian DGR are available (Briggs and Krol 2018). The expected bisulfide concentrations in a Canadian DGR are over an order of magnitude lower than 1 ppm, i.e., 30-90 ppb (Gascoyne 1997; Kremer 2017). The UFC surface was also modelled as a constant concentration boundary condition with a value of 0 ppm, which assumed that MIC occurs instantaneously at the UFC surface (Briggs and Krol 2018) (Figure 7c). The model used a finer mesh around the UFC to effectively capture the bisulfide diffusion in the region of interest, and a progressively larger mesh was applied towards the host rock to reduce computational cost. The hemispherical UFC end cap was meshed with extremely fine mesh due to its complex geometry. Triangular meshing was used in the 2-D model and tetrahedral meshing was used in the 3-D model (Briggs et al. 2017) and a total of 12,850 and 551,500 elements were used in the 2-D and 3-D models respectively (Figure 7d).

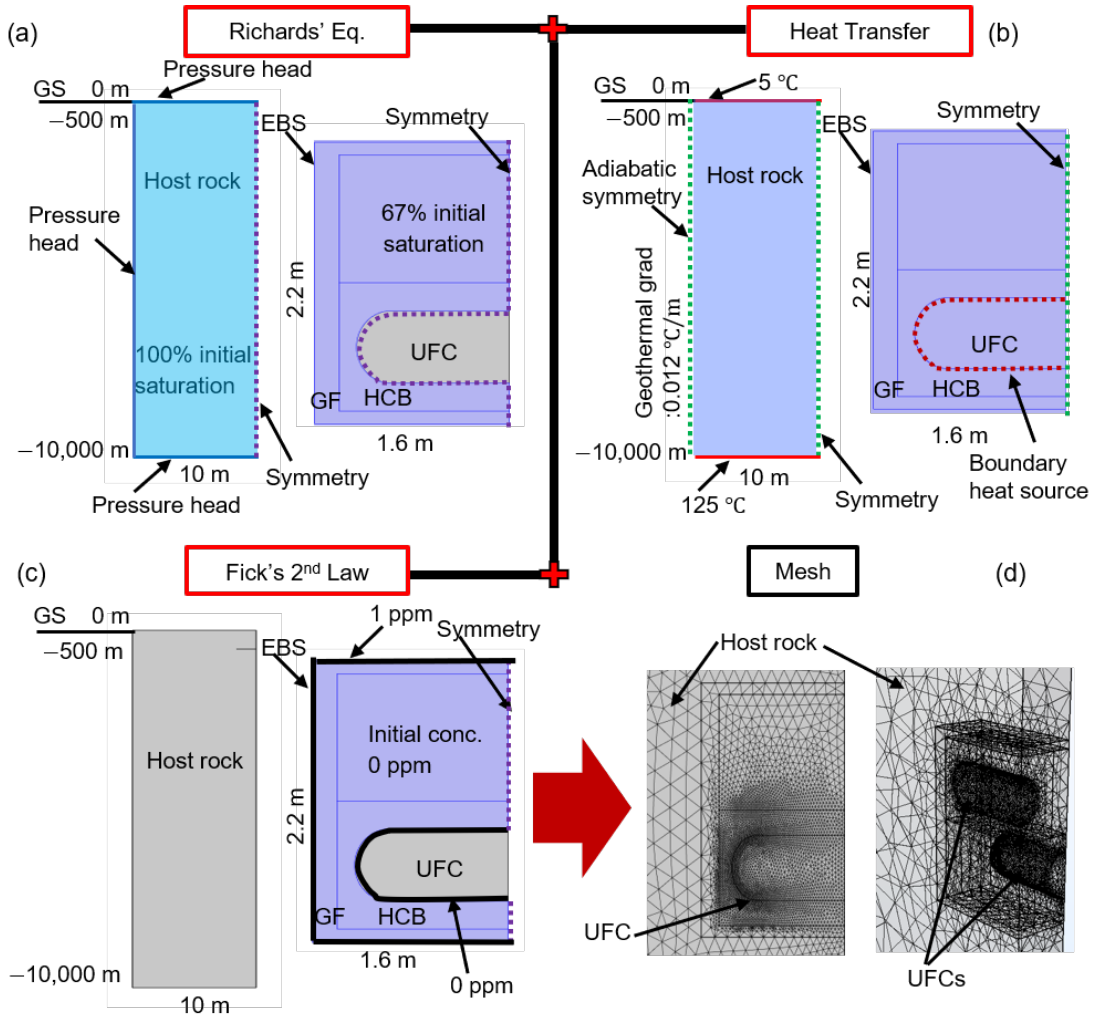

Figure 7: Initial and Boundary Conditions of the THC Model for: (a) Hydraulic (Richard's Equation), (b) Thermal (heat transfer), (c) Chemical (Fick's 2nd law), and (d) 2-D Triangular Mesh, and 3-D Tetrahedral Mesh. Note that the Geothermal Gradient and Boundary Temperatures in the Thermal Module are Shown for the Crystalline Domain.

3.2 PARAMETERS

Table 2 shows the model parameters obtained from (Gobien et al. 2016; Baumgartner 2006; Guo 2016, 2018; Gobien et al. 2018; SKB 2010; COMSOL 2021; Sykes et al. 2011; Dixon 2019; Dixon et al. 2018). These parameters represent the properties of groundwater, bisulfide, bentonite, UFC, and host rock.

Table 2: Model Parameters

Parameter	Domain	Value
General parameters		
Water, Air	All	Thermophysical properties from COMSOL 5.6 Material Library[1]
Hydraulic parameters		
Saturated liquid volume fraction[1]	HCB	0.382 (porosity)
Residual liquid volume fraction		0.001
Initial pressure head[2,3,4]		-8144.58 m in the crystalline DGR (67% initial in place average saturation)
		-10536.37 m in the sedimentary DGR (67% initial in place average saturation)

Permeability[3,4,5,6]		HCB	6 ×10^{-21} m^2 (crystalline groundwater)
			1 ×10^{-19} m^2 (sedimentary groundwater)
		Rock	4.08 ×10^{-17} m^2 (crystalline, average)
			2 ×10^{-21} m^2 (sedimentary, horizontal)
			2 ×10^{-22} m^2 (sedimentary, vertical)
Van Genuchten properties[3,4,8]	α	HCB	0.00022 m^{-1} (crystalline DGR)
			0.0000908 m^{-1} (sedimentary DGR)
	n		1.5 (crystalline DGR)
			2.71 (sedimentary DGR)
	m = 1-1/n		0.333 (crystalline DGR)
			0.63 (sedimentary DGR)
Thermal Parameters			
Density[2,7]		HCB	1700 kg m^{-3}
		Rock	2700 kg m^{-3}
		UFC	7750 kg m^{-3}
Thermal conductivity[4,5,7,8]		HCB	1.2 W/m K
		Rock	3 W/m K (crystalline)
			2.48 W/m K (sedimentary)
		UFC	60.5 W/m K
Specific heat[2,4,5,7]		HCB	1460 J/kg K
		Rock	845 J/kg K (crystalline)
			603.7 J/kg K (sedimentary)
		UFC	434 J/kg K
Surface temperature[2,7]		Rock	5 ˚C (crystalline)
			10 ˚C (sedimentary
Thermal gradient[2,7]			0.012 ˚C/m (crystalline)
			0.0103 ˚C/m (sedimentary)
Chemical Parameters			
Bisulfide concentration		Rock-bentonite interface	1 ppm (conservative assumption)
Bisulfide diffusion coefficient in water[9]		HCB	1× 10^{-9} m^2/s

[1]COMSOL (2021), [2]Gobien et al. (2016), [3]Baumgartner (2006), [4]Dixon et al. (2018), [5]Dixon (2019) [6]Sykes et al. (2011), [7]Guo (2016, 2018), [8]Gobien et al. (2018), [9]SKB (2010).

3.3 CONVERGENCE AND REPEATABILITY

Iterative convergence and mesh convergence were performed to ensure the model was properly discretized. Since the model simulates multiple coupled nonlinear processes, the iterative convergence value is important to ensure that errors do not propagate throughout the solution (An et al. 2011; Patankar 2018) . Iterative convergence is achieved by setting a relative tolerance/error criterion so that the error between current and previous iteration stays below the relative tolerance/error of the solver (i.e., $\frac{\text{Current iteration-Previous iteration}}{\text{Previous iteration}} < \text{relative tolerance}$). This is a self-correction method where the error calculated from the previous iteration is corrected by later iterations to reach at a solution, which is close to the exact solution (Logan 2007). For this model, the COMSOL solver was set with a relative tolerance of 10^{-5} to get repeatable results (i.e., the same result in different runs of the solver). Reducing the relative tolerance increased the solution accuracy (due to increasing iterations with smaller timesteps) but also increased the computation time. A relative tolerance of 10^{-5} was heuristically found to provide good repeatability at a reasonable computational time. A mesh convergence study was also performed to ensure the model was sufficiently discretized in space. This was done by changing the minimum element size and examining the maximum MIC rate. As seen in Figure 8, maximum MIC rates do not vary significantly for element sizes less than 0.05 m and therefore 0.01 m was chosen as the minimum element size.

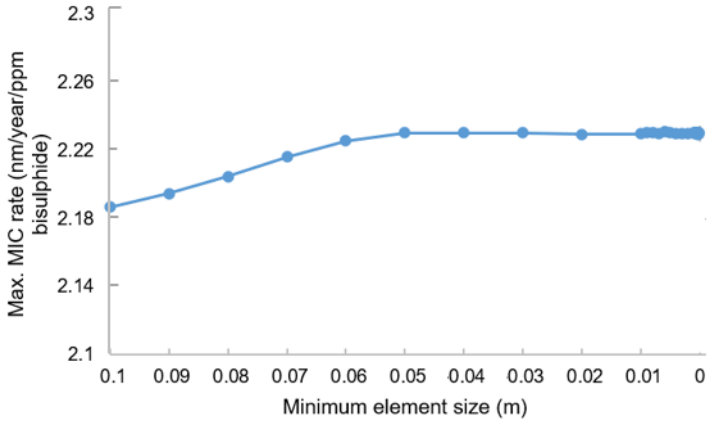

Figure 8: Mesh Convergence Study Showing the Change in Maximum MIC with Various Minimum Element Sizes.

3.4 MODEL CONFIRMATION

The mass transport and thermal processes have been verified by Briggs and Krol (2018) and the hydraulic process (Richard's equation) verification is presented here. As no 2-D experiments have been completed, the saturation process was verified by developing a 1-D saturation model that reproduced a quasi-1-D water infiltration experiment into clay (Figure 9). The 1-D saturation model used similar initial and boundary conditions compared to the THC model. The measured experimental infiltration data were taken from the unsaturated soil hydraulic database (UNSODA) (Nemes et al. 2001) and Moore (1939). The UNSODA data were fitted in the Microsoft Excel Solver to get the van Genuchten constitutive properties for the infiltration experiment, which were used as inputs in the 1-D saturation model.

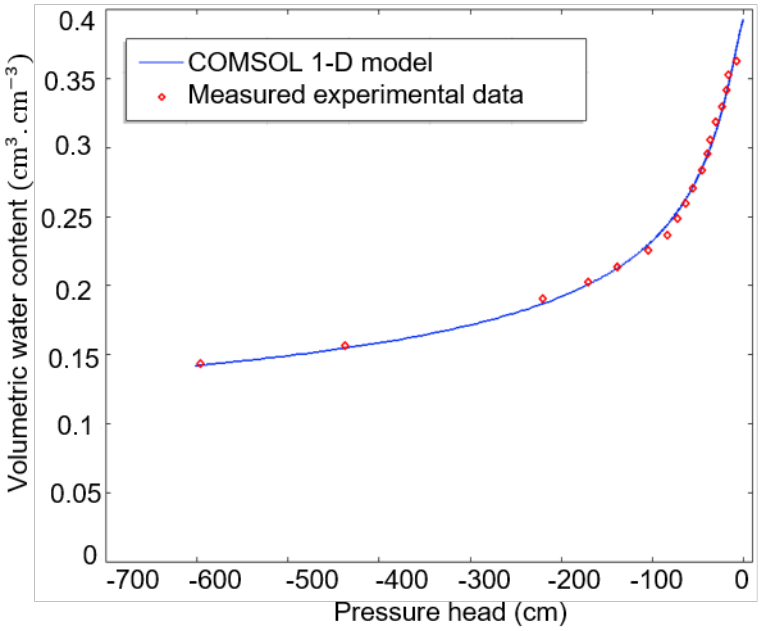

Figure 9: Comparison of Experimental Data from the Unsaturated Soil Hydraulic Database and a 1-D Saturation Model Developed Using the Richards' Equation in COMSOL.

4 MODEL RESULTS

4.1 MODEL IMPLEMENTATION AND SENSITIVITY STUDY

This section discusses sensitivity of the THC model to different boundary conditions, such as domain depth (section 4.1.1), pressure boundary conditions (section 4.1.2), and heat source implementations (section 4.1.3). These sensitivity analyses were done on the crystalline domain for the 2-D model and highlight characteristic trends that could be extended to the results in a 3-D domain.

4.1.1 Domain Depth

Identifying an optimal model domain depth is important to minimize both boundary effects and computation time. The model's domain needs to be large enough to avoid boundary effects, specifically those relating to groundwater flow and UFC heat dissipation.

Since the THC model used a constant temperature bottom boundary condition; it was important to set this boundary far below the UFC at a depth that did not affect UFC heat dissipation. When the bottom boundary was set too close to the EBS (i.e., 10 m below the EBS in the 510 m model) the model underpredicted UFC temperatures (with a maximum temperature close to 60 ˚C) (Figure 10a). This is because the constant temperature boundary condition forced an unrealistically high thermal gradient (Eq. 3) toward the bottom boundary, which cooled down the UFC.

On the other hand, this false cooling was not observed when the bottom boundary was set far from the EBS (i.e., in 1,000 m and 9,500 m below the EBS in the 1,500 m and 10,000 m models, respectively). In these models, the UFC temperatures rose to the expected values (i.e., up to maximum temperatures above 80 ˚C, Figures 10b and 10c). Thus, this sensitivity study showed that a proper domain depth was needed to minimize boundary effects and provide accurate temperature estimates. However, the 10,000 m domain was used in the model as UFC heat dissipation was slower compared to the 1,500 m domain (Figure 11). In addition, the 10,000 m deep model is comparable to other developed DGR models (e.g., Guo, 2016). It is important to note that the second temperature "bump" in the 1,500 and 10,000 m models (Figure 11) is due to the heat symmetry boundary condition and is not representative of the true temperature in the DGR. See additional commentary on this phenomenon in Guo (2016).

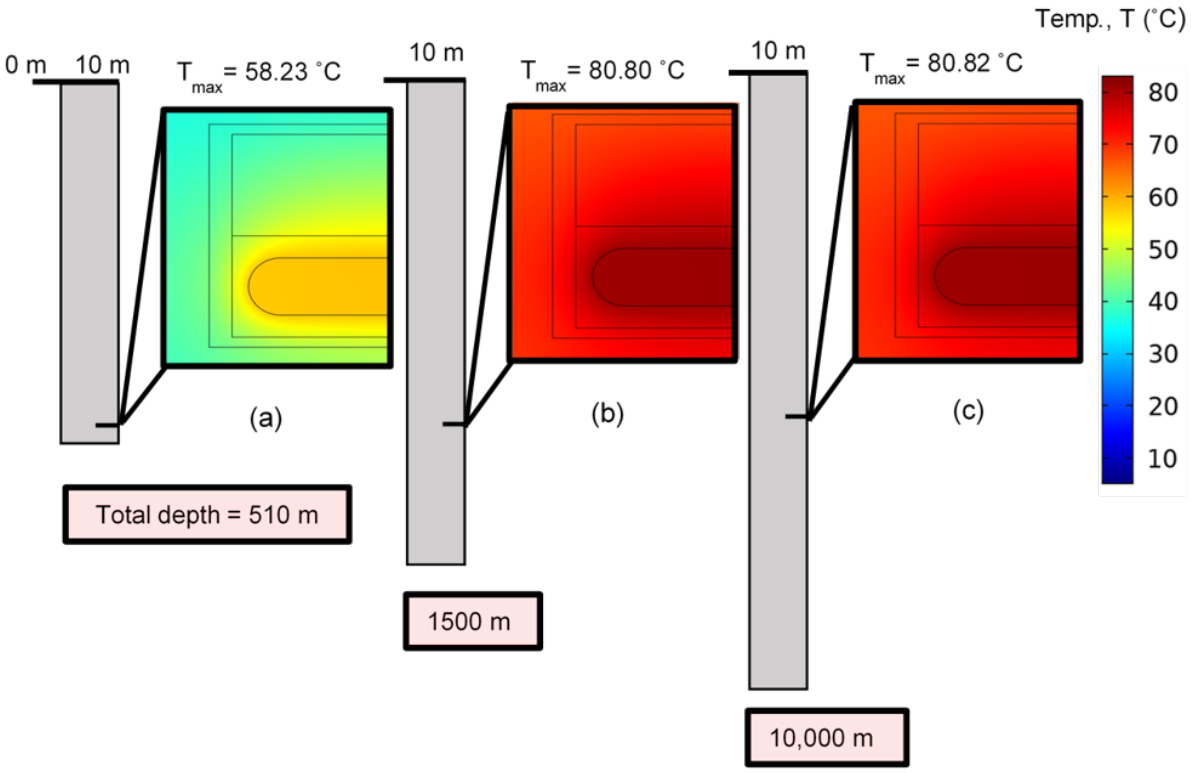

Figure 10: Domain Depth Sensitivity, (a) Boundary Effect: Placing Bottom Boundary 10 M Below the EBS Underpredicted the UFC Temperature, (b & c) UFC Temperature Rose to the Expected Value (i.e., Maximum Temperature Above 80 ˚C) When Bottom Boundary was Moved Away From the EBS. Note That the Figures are not to Scale.

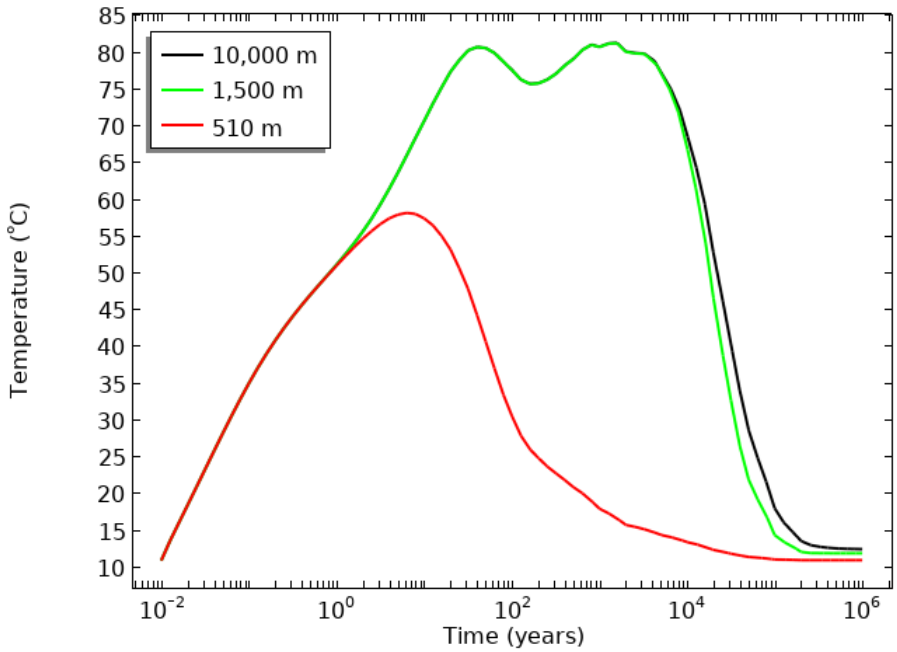

Figure 11: Temperature profiles in different depth models.

4.1.2 Pressure Boundary Conditions

The original model developed by Briggs and Krol (2018) used a Type 2 (no-flow) boundary condition. This boundary condition meant that no water entered the system during saturation,

which created an anomalous low-pressure region at late-times (e.g., after 630 years in Figure 12a). Therefore, Type 1 (pressure head) boundary conditions were implemented for the current model (Figure 12b). Type 1 boundary conditions resulted in a decreased time to full saturation (from approximately 2000 to 20 years) as water was able to enter the model domain from the boundaries. Although this phenomenon is dependent on soil pressure-saturation parameters, the resulting pressure build up is a common result when using the no flow boundary conditions. Therefore, the constant head boundary condition is a better representation of the expected DGR behaviour during saturation.

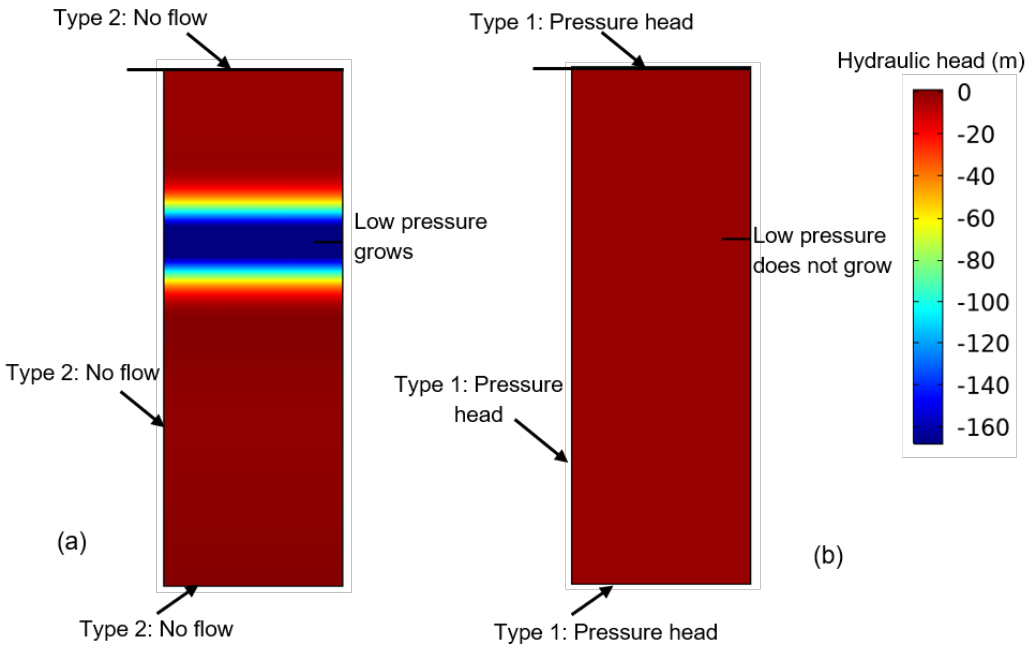

Figure 12: Flow Boundary Conditions Sensitivity for: (a) Type 2: No Flow Boundary Conditions (b) Type 1: Pressure Head Boundary Conditions. Results are Shown at 630 Years.

4.1.3 Heat Source

The heat output from the UFC (Tait et al. 2000) can be implemented into COMSOL over a boundary or a domain. For the 2-D model, a boundary heat source (Figure 13a) was compared to a domain heat source (Figure 13b), and it was found that the latter overpredicted the UFC temperature. This overprediction occurred because the domain heat source was distributed over a 3-D volume and when applied to a 2-D model it overpredicted the heat flux throughout the selected domain. In comparison, when the heat source boundary defined the flux over the selected boundary (area), the 2-D model better approximated the anticipated heat flux into the domain.

In the 3-D model, the heat flux was defined over the 3-D volume using a UFC heat rate that is divided by the UFC volume. This correctly approximated the anticipated heat flux into the domain and the temperature output aligned well with expected results (Guo, 2017).

The discrepancies described in these sections, highlight how slight differences in model assumptions can lead to errors or inaccurate results; therefore, boundary conditions and initial conditions need to be chosen carefully.

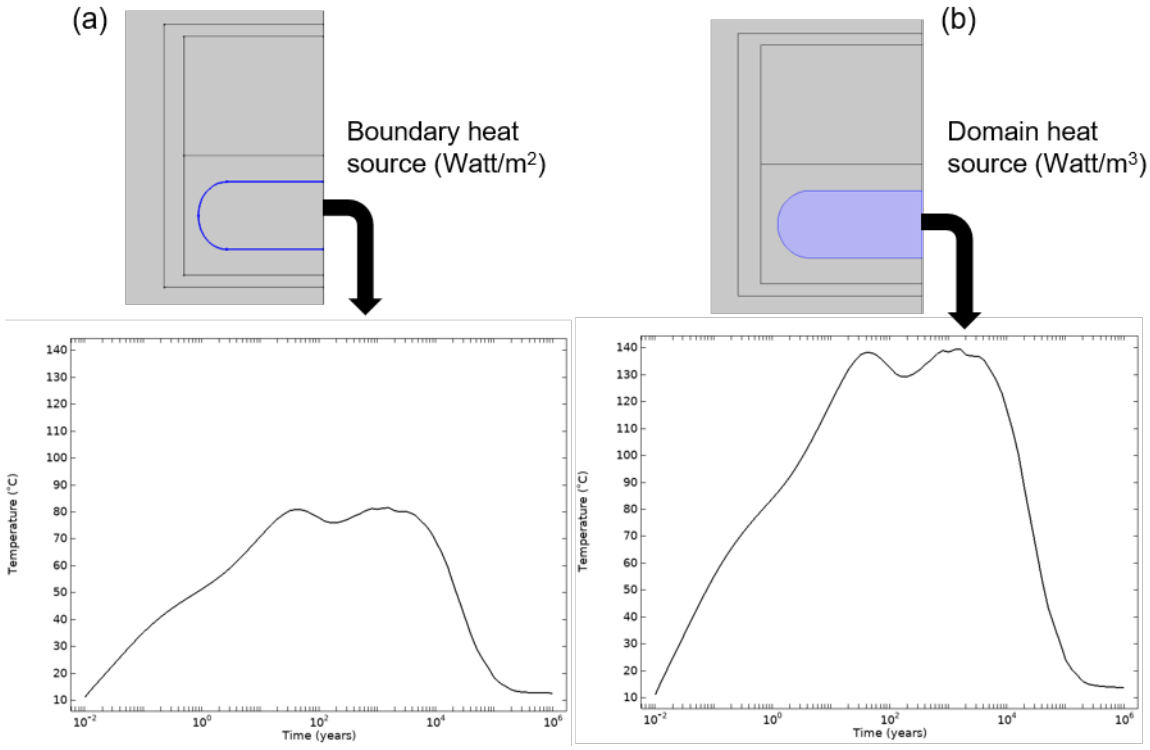

Figure 13: Heat Source Sensitivity Using a: (a) Boundary Heat Source, and (b) Domain Heat Source for a 2-D Model. Total Domain Depth of 10,000 M was Used in both Cases.

4.2 SATURATION TIME

The 2-D THC model was run for a reference period of 1 million years with an initial bentonite saturation of 67% and fully saturated rock. Figure 14 shows water saturation in the crystalline DGR after 2, 5, and 15 years. The HCB near the hemispherical ends of the UFC saturates first within 5 years. Full saturation occurs after 20 years for a host rock permeability of $4.08\times10^{-17}m^2$(reference case for the crystalline rock, Table 2). This result compares well with other studies assuming similar host rock conditions, i.e., 10's-100's of years (Millard et al. 2004; Nguyen and Jing 2005). Saturation evolution in the sedimentary DGR is slower than the crystalline DGR, as seen in Figure 15 due to lower rock permeability. In addition, the saturation front is not as pronounced in the sedimentary DGR due to the relative permeability of the rock with respect to bentonite. In the crystalline domain, the rock has a higher permeability compared to bentonite while in the sedimentary DGR the rock has a lower permeability (Table 2). However, since the rock permeability in the sedimentary domain is lower than in the crystalline, full saturation occurs later - after 160 years for a host rock horizontal permeability of $2\times10^{-21}m^2$ and vertical permeability of $2\times10^{-22}m^2$ (reference case for the sedimentary rock, Table 2). Capturing this difference in saturation evolution is important to delineate the oxic and anoxic corrosion. However, this saturation evolution may also be affected by other variables in the host rock, e.g., natural permeability heterogeneity, salinity, and excavation induced fractures.

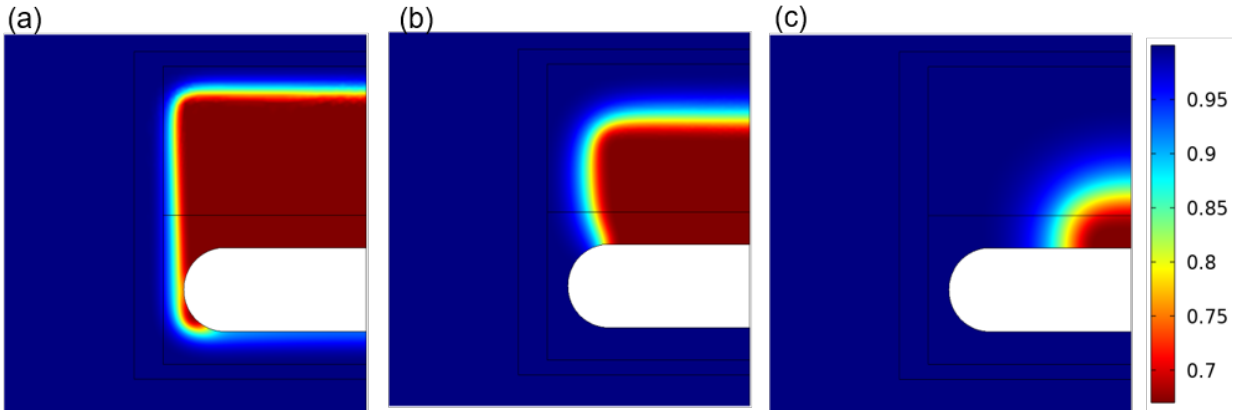

Figure 14: Water saturation in the Crystalline DGR after a) 2 Years, b) 5 Years, and c) 15 Years. Average Permeability of Rock and Bentonite are 4.08×10^{-17} m^2 and 6×10^{-21} m^2, Respectively.

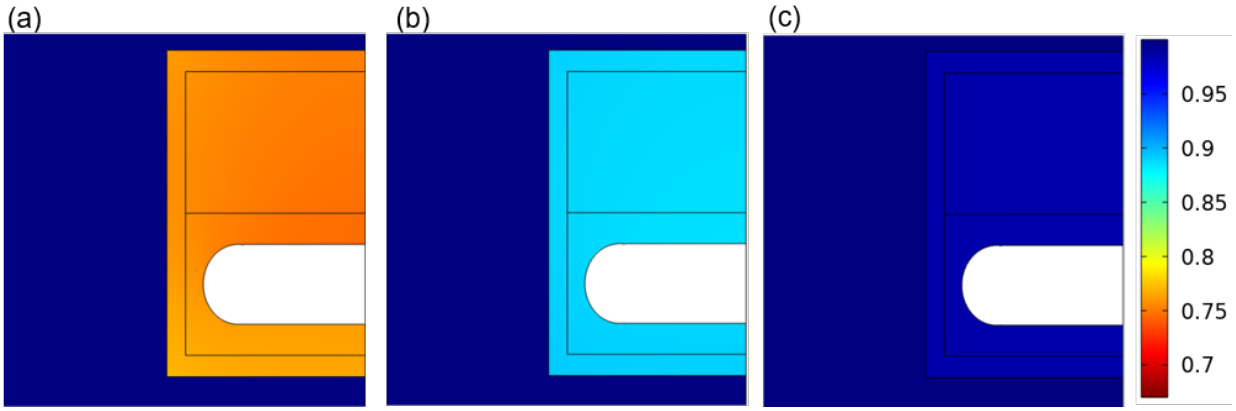

Figure 15: Water Saturation in the Sedimentary DGR After a) 15 Years, b) 50 Years, and c) 100 Years. Horizontal and Vertical Permeabilities of Rock are 2×10^{-21} m^2 and 2×10^{-22} m^2, Respectively. Average Bentonite Permeability is 1×10^{-19} m^2.

Figure 16 shows sensitivity in saturation profiles due to varying rock permeability. Typically, increasing rock permeability decreases bentonite saturation time. However, the saturation times are insensitive to the rock permeability when it is higher than the bentonite permeability. This insensitivity is seen in the saturation profiles in the crystalline DGR, which do not vary significantly with rock permeability of greater than 10^{-19} m^2 due to the lower bentonite permeability ($6\times10^{-21}m^2$, Table 2) and results in a consistent saturation time for all crystalline rock permeabilities (20 years, Figure 16a). In addition, saturation time will also be affected by the soil van Genuchten parameters which govern initial saturation condition and soil water characteristic curve of the bentonite (Van Genuchten 1980; Baumgartner 2006).

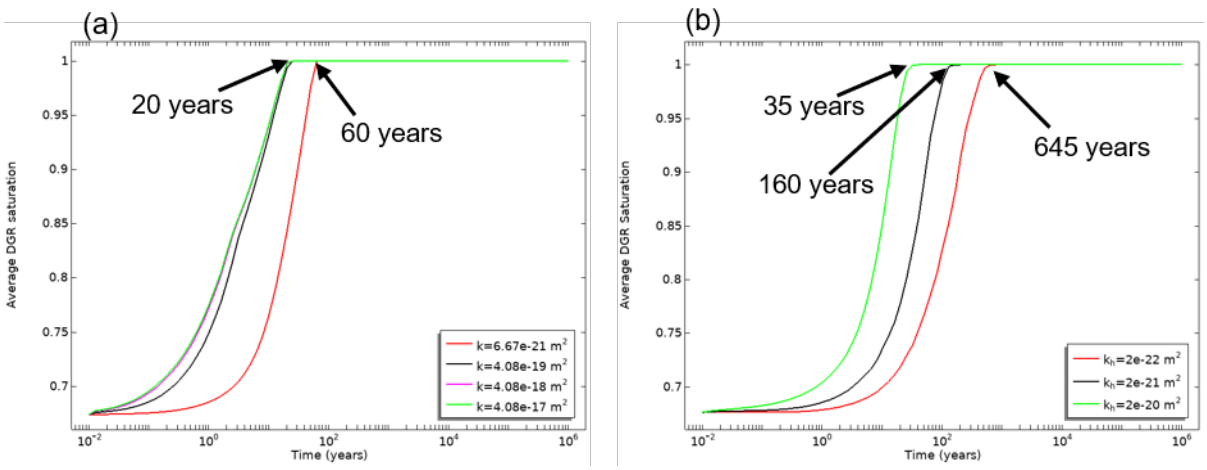

Figure 16: Average Water Saturation Over the Estimated Life Span of the DGR for Varying a) Average Permeabilities of the Crystalline Rock (bentonite k= 6×10^{-21} m^2), b) Horizontal Permeabilities of the Sedimentary Rock While Keeping the Vertical Permeability Unchanged (bentonite k= 1×10^{-19} m^2).

4.3 BISULFIDE FLUX AND MIC DEPTH

Bisulfide fluxes were examined in the crystalline DGR after 2, 5, and 15 years (Figure 17) and the sedimentary DGR after 15, 50, and 100 years (Figure 18). The effective bisulfide diffusion coefficient was kept at $1\times10^{-11}m^2\ s^{-1}$ in both models. The MIC depth, d_{corr} at a given time at the UFC is a function of bisulfide flux and Equation 1 and was calculated following SKB (2010):

$$d_{corr}=\frac{N_{HS}f_{HS}M_{cu}}{A_{corr}\rho_{cu}} \tag{11}$$

N_{HS}/A_{corr} is the bisulfide flux computed from the model, f_{HS} is the stoichiometric factor (with a value of 2 from the stoichiometry of Eq. 1), M_{cu} is the molar mass of copper, and ρ_{cu} is the density of copper. The MIC depth over time (i.e., MIC rate) can be calculated at the UFC. Initially, the MIC rate is zero since no bisulfide is present at the UFC. Bisulfide diffusion occurs from the host rock as the bentonite becomes saturated. More bisulfide enters through the bottom boundary (Figure 17a) as the sharp saturation front saturates the bentonite near the bottom boundary first compared to other parts (Figure 14a). The maximum bisulfide flux occurs at the hemi-spherical UFC end caps due to EBS and UFC geometry (Briggs et al, 2017). The maximum MIC rate in the crystalline DGR is 2 $nm.year^{-1}$ppm $bisulfide^{-1}$after 1653 years. The maximum MIC rate in the sedimentary DGR is 2.54 $nm.year^{-1}$ppm $bisulfide^{-1}$after 1267 years. It is important to note that the MIC rate is solely based on bisulfide diffusion and not on the rate of bisulfide production due to SRB activity (microbial reactions are not considered in this model). Thus, all of these calculations may be considered conservative.

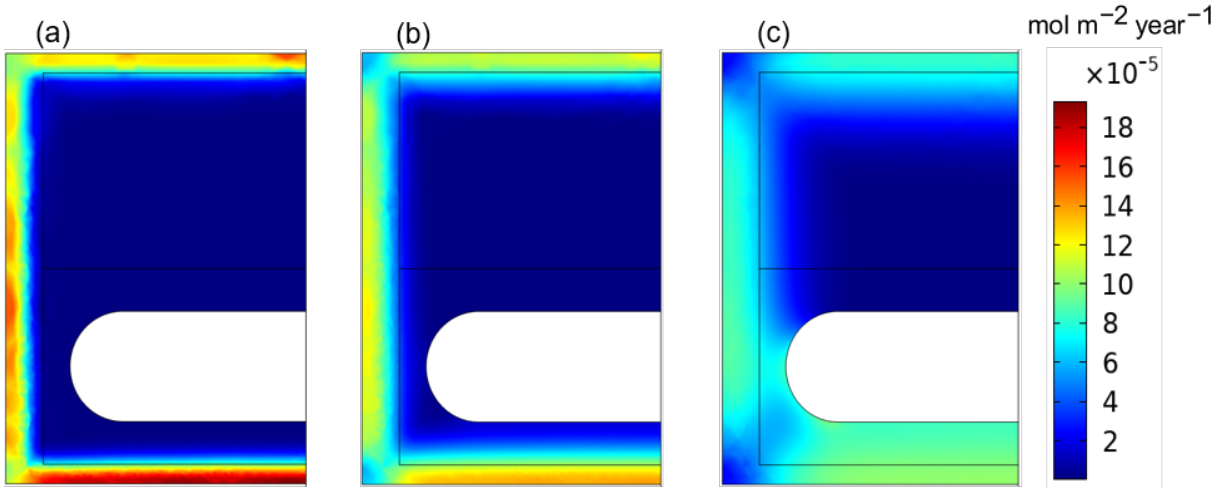

Figure 17: Bisulfide Flux in the Crystalline DGR after a) 2 Years, b) 5 Years, and c) 15 Years.

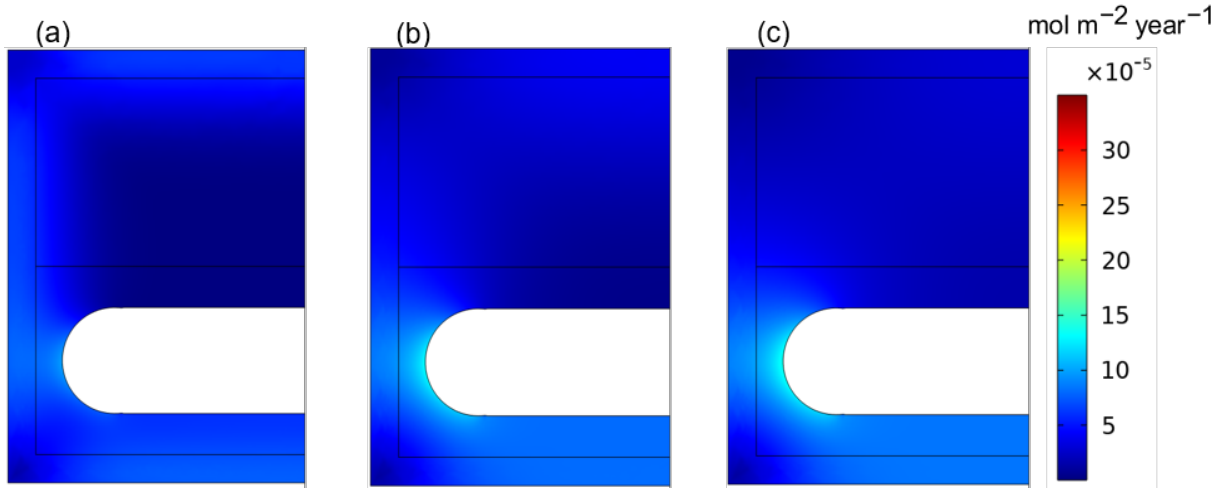

Figure 18: Bisulfide Flux in the Sedimentary DGR after a) 15 Years, b) 50 Years, and c) 100 Years.

4.4 CURRENT MODEL VERSUS PREVIOUS MODELS

The previous study (Briggs and Krol 2018) assessed the effects of saturation and temperature on MIC using separate models. These models simulated: (*i*) Chemical (Diffusion) processes (referred to as the "C model", Figures 19a, and 20a), (*ii*) Hydraulic-Chemical (Diffusion) processes (referred to as the "HC model", Figures 19b, and 20b), and (*iii*) Thermal-Chemical (Diffusion) processes (referred to as the "TC model", Figures 19c, and 20c). This current work (the "THC model", Figures 19d, and 20d) explores the combined effects of saturation, diffusion, and temperature in one model, to improve MIC estimations.

Figure 19e compares maximum MIC rates from different models set in the crystalline DGR. As the bisulfide diffusion rate is dependent on saturation and temperature (Eqs. 5, and 6), the MIC rate is also controlled by hydraulic and thermal conditions. In the TC model, bisulfide enters the system after year "one" and the diffusion rate increases with temperature (Figures 19c, and e). In comparison, bisulfide transport starts later in the HC model (approximately 3 years) and the THC model (approximately 1.5 years) once water has infiltrated the bentonite (Figures 19b, d, and e). Bisulfide transport starts after 3 years in the C model as temperature does not affect the

diffusion rate in an isothermal system (Figures 19a, and e). Therefore, bisulfide travel time is mostly affected by temperature, followed by saturation of the system in the crystalline domain.

All models reach steady-state MIC rates when UFC heat has fully dissipated, and temperature returns to the background level (approximately after 2 × 10^5 years). MIC rates in TC and THC models are very similar (Figure 19e) as saturation in the THC model is fast (Figure 14) and does not significantly delay the onset of bisulfide diffusion. In addition, the total MIC depth as estimated using Equation 11 (Table 3), shows that the MIC rates with and without variable saturation (i.e., THC vs. TC) are also nearly identical, whereas the MIC rate in isothermal conditions are lower showing that temperature has a bigger impact on bisulfide diffusion than saturation in the crystalline domain. It should be noted that these MIC estimates are conservative as these models assume there is no sorption or reactions within the bentonite, no evaporation or gaseous transport is simulated, and bentonite swelling is assumed to occur instantaneously (bentonite permeability is given for swelled conditions). In addition, the MIC estimates are conservative due to the second temperature “bump”, which is identified as a modelling artefact (see section 4.1.1).

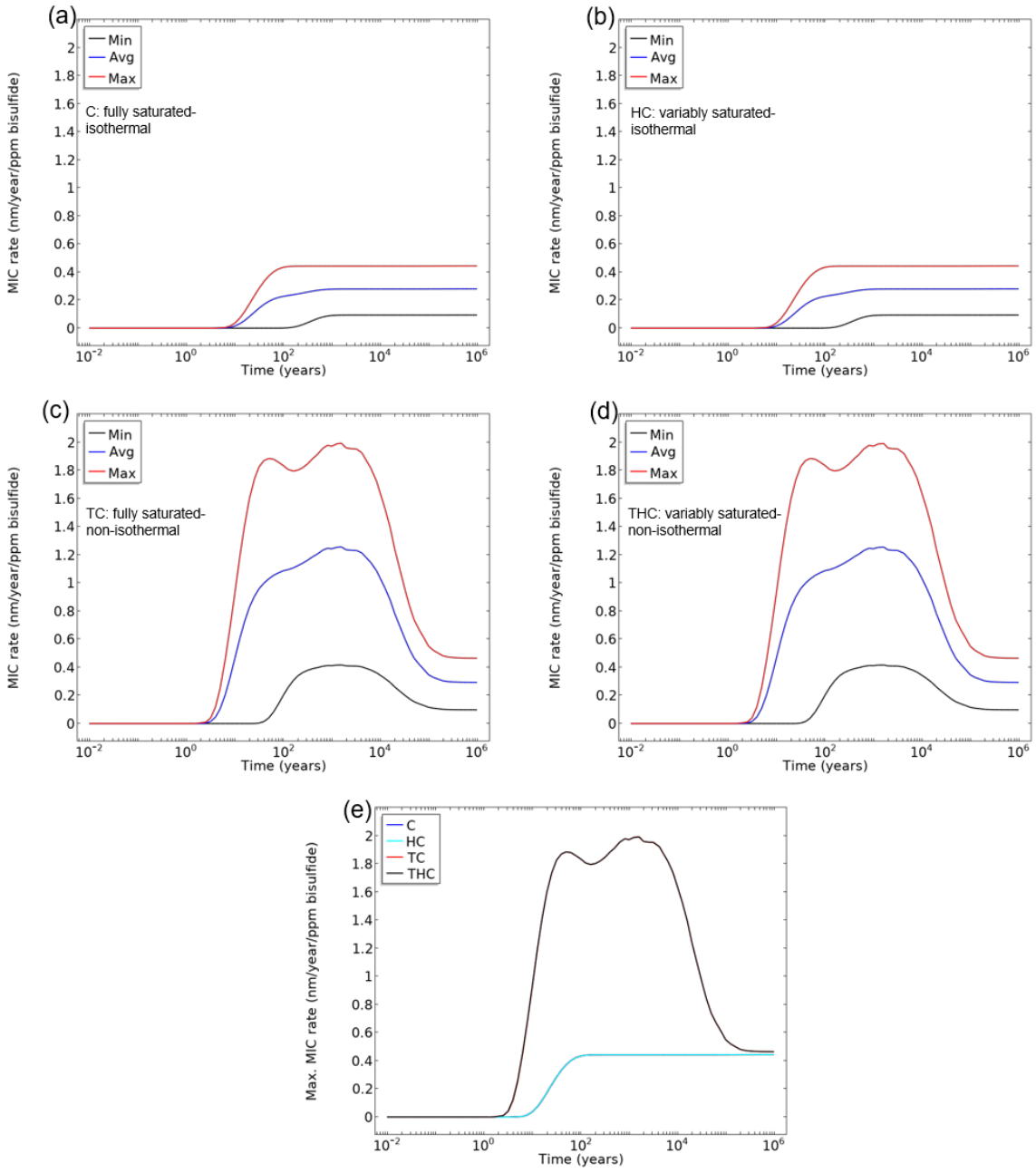

Figure 19: MIC Rates (Max, Min, Average) in the Crystalline DGR under Different Conditions a) C Model Simulates Bisulfide Diffusion Under Fully Saturated-Isothermal Conditions, b) HC Model Simulates Bisulfide Diffusion Under Variably Saturated-Isothermal Conditions, c) TC Model Simulates Bisulfide Diffusion Under Fully Saturated-non-isothermal conditions, d) THC Model Simulates Bisulfide Diffusion Under Variably Saturated-Non-Isothermal Conditions, and e) Maximum MIC Rates in all the Different Models.

Figure 20e compares maximum MIC rates from different models set in the sedimentary DGR. Like crystalline DGR, bisulfide enters the system after year “one” in the TC model and diffusion rate increases with temperature (Figures 20c, and e). In comparison, bisulfide transport starts later in the HC model (after ~5 years) and THC model (after ~2 years) after water has infiltrated the bentonite (Figures 20b, d, and e). Bisulfide transport starts after 2 years in the C model as temperature does not affect diffusion rate in an isothermal system (Figures 20a, and e). Unlike the crystalline domain, MIC rates in TC and THC models are different (Figure 20e) as saturation of the domain in the THC model delays the onset of bisulfide diffusion as it transports through the water filled fraction of the pore space; however, the peak MIC rates are similar (Figure 20e). The same is seen for the C and HC models (Figure 20e). Like the crystalline DGR, the total MIC depths (Table 3) are nearly identical for the THC and TC models, suggesting that the transient MIC rates last for a short time compared to the overall DGR lifespan.

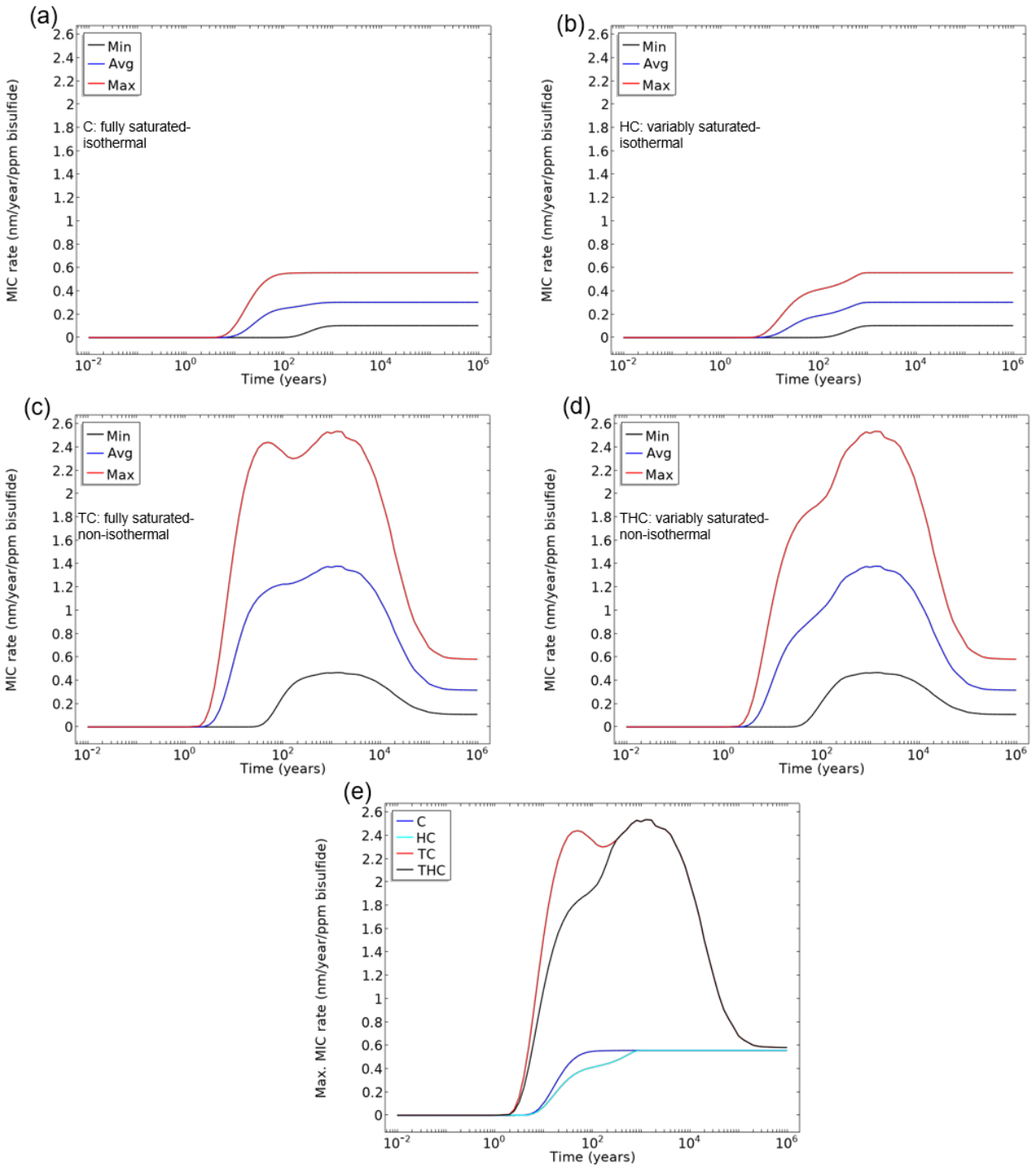

Figure 20: MIC Rates (Max, Min, Average) in the Sedimentary DGR Models Under Different Conditions a) C Model Simulates Bisulfide Diffusion Under Fully Saturated-Isothermal Conditions, b) HC Model Simulates Bisulfide Diffusion Under Variably Saturated-Isothermal Conditions, c) TC Model Simulates Bisulfide Diffusion Under Fully Saturated-Non-Isothermal Conditions, d) THC Model Simulates Bisulfide Diffusion Under Variably Saturated-Non-Isothermal Conditions, And E) Maximum MIC Rates in all the Different Models

Table 3: Total maximum MIC Depths Calculated by the Various Models

Model	Total maximum MIC depth (mm)	
	Crystalline	Sedimentary
C	0.443	0.556
HC	0.443	0.556
TC	0.517	0.645
THC	0.517	0.645

To demonstrate this, Figure 21 shows maximum MIC rates plotted against a linear time scale. This figure shows that the MIC rates driven by changes in saturation and UFC temperature (that impact bisulfide diffusion rates), only occur during the initial life span of the DGR (i.e., before 200,000-400,000 years). After this time, the DGR conditions are fully saturated and isothermal. Therefore, the comparisons in Figure 21 help to understand the relative importance of including different processes in the model and how the system behaves over time due to coupling these processes.

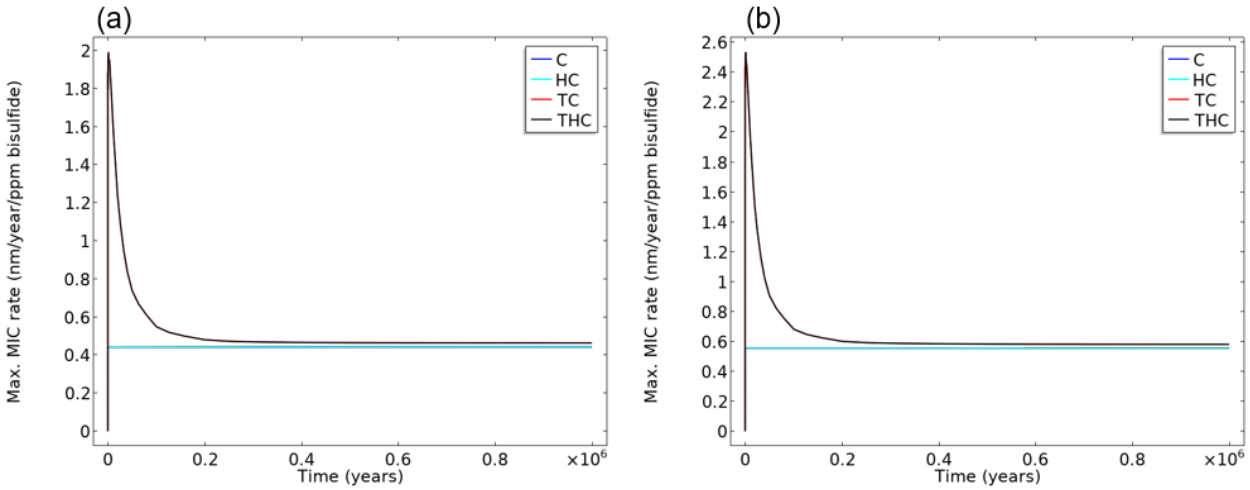

Figure 21: Maximum MIC Rates in Different Models, Plotted Against a Linear Time Scale, a) Crystalline DGR, and b) Sedimentary DGR

4.5 PREDICTED DGR ENVIRONMENTAL CONDITIONS

The THC model was also used to show the predicted environmental conditions and bisulfide flux distribution in the crystalline and sedimentary DGRs (Figure 22). The initial bentonite saturation is assumed to be 67% in both DGRs; however, full saturation occurs at different times due to the differences in rock permeability. The normalized gas content is approximated as a function of effective water saturation ($(1-S_e)/(1-S_{e,0})$), which is assumed to correspond to a passive gas phase with negligible gas pressure gradients. In other words, gas content decreases as water flows through pores due to water pressure head gradients. Therefore, these models do not simulate the free and dissolved gas mass balance or gas movement within the DGR. Instead, the influence of key physical processes affecting bisulfide flux (i.e., saturation and heating) are highlighted. The low degree of saturation lowers bisulfide flux (seen most clearly in Figure 22b), as bisulfide is assumed to transfer through the water-filled fraction in the pore space. The peak bisulfide flux occurs under high UFC temperatures when the DGR is fully saturated (Figure 22).

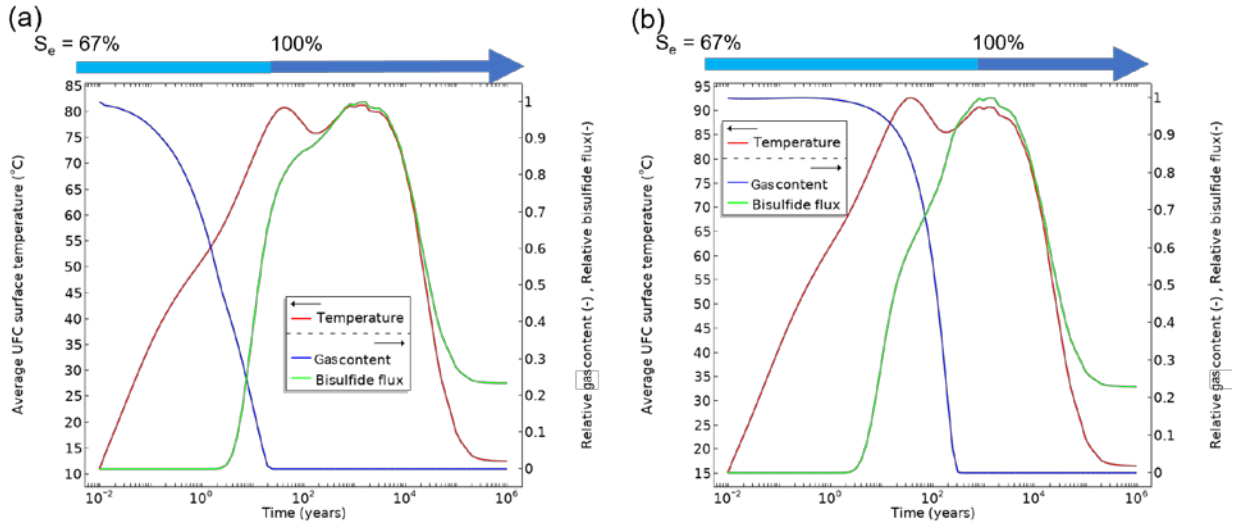

Figure 22: Predicted Environmental Conditions from the THC Models in the a) Crystalline DGR, and b) Sedimentary DGR. Note that the Average Bentonite Gas Content (passive gas phase) and Bisulfide Flux Values are Normalized.

5 3-D THC MODEL

The previous results were given for the 2-D model therefore Figure 23 compares maximum MIC rates, temperature, maximum bisulfide flux, and average DGR saturation in the 2-D and 3-D THC models set in the crystalline DGR. As seen in Figure 23a, maximum MIC rates in the 2-D and 3-D THC models are not the same. The total MIC depth in the 3-D THC model is 0.671 mm while the 2-D THC model estimates 0.517 mm (Table 3). This difference occurs due to 3-D geometry (also observed by Briggs and Krol (2018)), which captures MIC rates in the third dimension that are not included in the 2-D model. However, the characteristic UFC temperature (Figure 23b) and degree of saturation (Figure 23c) are very similar between the 2-D and 3-D models. In addition, the trends and sensitivities discussed in Section 4 are the same for the 2-D and 3-D models. The effects of governing transport mechanisms on MIC are explored using a 3-D model in Rashwan et al. (2022).

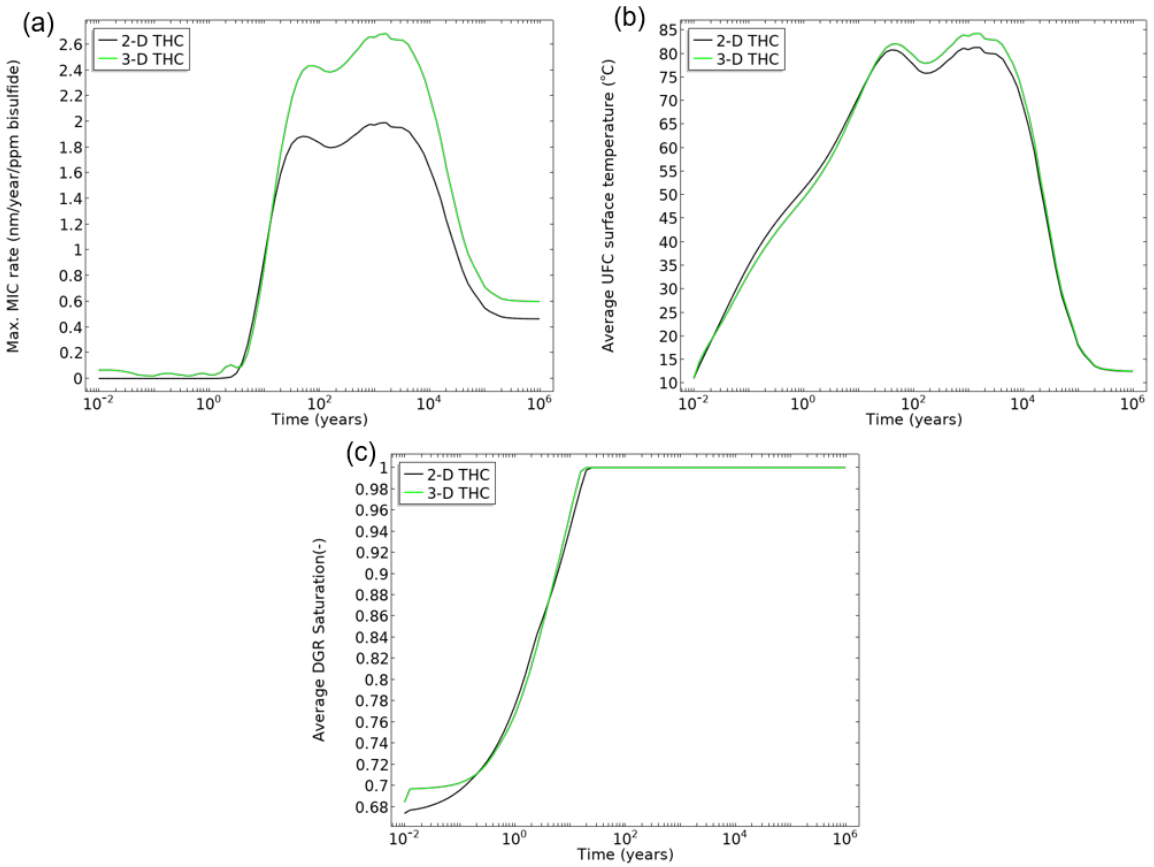

Figure 23: 2-D THC Versus 3-D THC Models of the Crystalline DGR, a) Maximum MIC Rates, b) Temperature, and c) Average DGR Saturation.

6 THEORETICAL AND NUMERICAL BISULFIDE FLUX

Figure 24 compares bisulfide fluxes from a simplified 1-D analytical and 1-D, 2-D, and 3-D numerical C models, set in the crystalline DGR. The 1-D models consider the transient diffusion from the centre of the UFC end cap to the rock-bentonite interface. As seen in Figure 24, bisulfide fluxes from the 1-D analytical and 1-D numerical models are identical. In addition, bisulfide fluxes from the 2-D and 3-D numerical C models match well with the 1-D analytical flux in the early times (i.e., during the first 30 years). The early matching reveals that the onset of bisulfide diffusion occurs through 1-D transport path (i.e., the shortest distance from the rock-bentonite interface to the UFC end cap/caps). The difference in bisulfide fluxes after 30 years indicates multidimensional transport, which was not considered in the 1-D analytical model. Therefore, the similarity in bisulfide evolution in the analytical and numerical models further confirms that the numerical approximation used in the DGR models is appropriate and the model is properly developed.

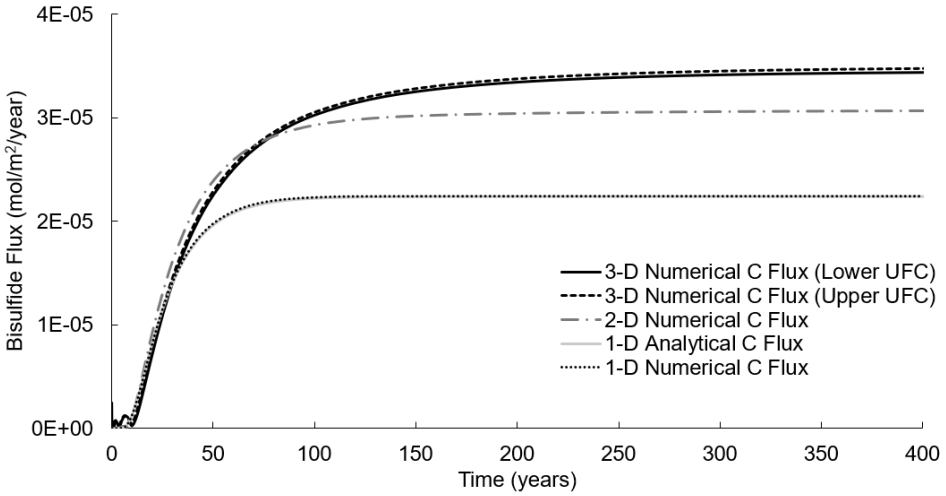

Figure 24: Comparison of Bisulfide Fluxes from an Analytical Model and Numerical C Models of the Crystalline DGR.

7 DISCUSSION AND FUTURE WORK

This report outlines the long-term conditions anticipated in the DGR, conceptual models of the processes affecting MIC, and results of the newly coupled 2-D and 3-D Thermal-Hydraulic-Chemical (Diffusion) model (referred to as the "THC model"). The THC model can simulate bisulfide diffusion through the bentonite in the DGR under variably saturated and non-isothermal conditions. Moreover, the specific implementation and verification procedures have been documented. The parameters used in the model are obtained from NWMO case studies (Gobien et al. 2016, 2018; Sykes et al. 2011; Dixon 2019; Dixon et al. 2018; Guo 2016, 2018), and other sources (Baumgartner 2006; SKB 2010). This model is designed to be flexible and accommodate site-specific information as it becomes available; however, many of the key trends elucidate characteristic evolution expected in the DGR and its influence on MIC.

A range of verification and validation procedures were conducted to develop confidence in the THC model. For example, a mesh convergence study was performed to ensure the model was properly discretized in space. In addition, a sensitivity study on various boundary conditions was performed to ensure boundary assumptions were not leading to spurious, unrealistic results. A domain depth of 10,000 m was used as it provided the expected temperature profile without increasing computational time. In addition, constant pressure head conditions were used at the model flow boundaries to simulate realistic flow conditions and avoid anomalous low-pressure zones that developed at late-times with no-flow boundaries. Around the UFC, a boundary heat source was chosen to model the heat generated by the used nuclear fuel, as a domain heat source overpredicted the UFC temperature due to geometry and modelling inputs. The host rock was assumed to be fully saturated, the HCB was initially at 67% saturation and a constant, 1 ppm bisulfide concentration boundary condition was assumed at the rock-bentonite interface. The 2-D THC model was compared with previous models developed by Briggs and Krol (2018) and the 3-D THC model was developed and compared with the 2-D THC model and two 1-D C models (analytical and numerical) for verification purposes. Lastly, the robustness of the numerical approximation used in the model was confirmed through good agreement between numerical and theoretical solutions.

The mass transport and thermal processes were validated by Briggs and Krol (2018), while the hydraulic process (Richard's equation) verification is presented in this report. As no 2-D experiments have been completed, the saturation process was verified by developing a 1-D saturation model which reproduced a quasi-1-D experiment of water infiltration into clay. Upon verification, the THC model was run for both DGR domains and it predicted 20 years and 160 years for full saturation in the crystalline and sedimentary host rock models, respectively. These saturation times are comparable to the results from other HCB saturation studies assuming

similar host rock conditions, i.e., 10's-100's of years (e.g., DECOVALEX III project results). Bentonite saturation is slower in the sedimentary rock compared to the crystalline rock due to lower rock permeabilities. In addition, the saturation front is not as sharp in the sedimentary domain due to the relative magnitude of permeability of the rock and bentonite. Typically, increasing rock permeability would decrease bentonite saturation time. However, the saturation times are insensitive to rock permeability when the rock permeability is higher than the bentonite permeability, making the bentonite the governing transport layer (as seen in the crystalline domain).

Capturing this difference in saturation evolution is important to delineate the oxic and anoxic corrosion. However, this saturation evolution may be affected by many variables in the host rock and bentonite, e.g., permeability, salinity, and excavation induced fractures. The estimation of saturation time is also controlled by the van Genuchten parameters which govern initial saturation condition and soil water characteristic curve of the bentonite.

This report also provides a model comparison between the THC model and previous models developed by Briggs and Krol (2018)). This analysis reveals that the MIC is driven by changes in saturation and UFC temperature that impact bisulfide diffusion rates, which only occurs during the initial life span of the DGR (i.e., before 200,000 - 400,000 years). After this time, bisulfide diffusion occurs in a saturated system under isothermal conditions. In addition, the 3-D THC model, set in the crystalline DGR, results in a total MIC depth of 0.671 mm, compared to 0.517 mm using the 2-D THC model. This difference in MIC depths is due to the 3-D geometry which includes bisulfide flux from an additional dimension and shows the importance of using 3-D simulation to estimate corrosion depth.

As bisulfide transport is diffusion dominated, and no gaseous transport is assumed, bisulfide transport starts as the EBS pore space becomes saturated. The maximum bisulfide flux occurs at the hemi-spherical end caps of the UFC as water contacts the caps first due to UFC and EBS geometry. The total maximum MIC depths are 0.645 mm and 0.517 mm in million years in the sedimentary and crystalline DGR, respectively. However, this MIC estimate is conservative due to several assumptions, such as:

- no sorption, geochemical reactions or microbial processes are assumed to be occurring within the bentonite; including these reactions would decrease the amount of bisulfide that would be transported to the UFC
- bentonite is assumed to swell instantly, and bentonite permeability is assumed to be constant throughout the simulation; including bentonite swelling may increase bisulfide transport in the early times due to higher bentonite permeability; this would have a bigger impact in the crystalline domain as the bentonite permeability has a more controlling impact on diffusion
- No vapour transport or evaporation or condensation is modelled in the system; including these processes would lead to cooling of the system resulting in lower bisulfide transport

In summary, the THC model has been robustly developed to aid in the performance assessment of the Canada's DGR. The developed THC model is designed to be flexible to accommodate additional processes and site-specific information as it becomes available. Future work will include sorption and geochemical reactions, vapour transport, bentonite swelling, corrosion equations, microbial reactions, and biochemical modelling.

ACKNOWLEDGEMENTS

This research is supported by NWMO, NSERC, and ORF who provide funding through York University.

REFERENCES

An, W., T. Zhu and L.-J. Yin. 2011. Improved iterative convergence of the finite element method in the solution of the second-order radiative transfer equation by modified diffusion synthetic acceleration. Numerical heat transfer, Part B: Fundamentals, 59, 409–420.

Avis, J., R. Walsh and N. Calder. 2012. Corrosion-Generated Hydrogen Gas from Steel Used Fuel Containers and the Postclosure Pressure within a Deep Geological Repository. Nuclear Waste Management Organization Report APM-03640-T10. Toronto, Canada.

Baumgartner, P. 2006. Generic Thermal-Hydraulic-Mechanical (THM) Data for Sealing Materials, Volume 1: Soil-Water Relationship. Atomic Energy of Canada Ltd. Report AECL-06819. Pinawa, Canada.

Briggs, S. and M. Krol. 2018. Diffusive Transport Modelling of Corrosion Agents through the Engineered Barrier System in a Deep Geological Repository for Used Nuclear Fuel. Nuclear Waste Management Organization Report NWMO TR-2018-06. Toronto, Canada.

Briggs, S., J. McKelvie, B. Sleep and M. Krol. 2017. Multi-dimensional transport modelling of corrosive agents through a bentonite buffer in a Canadian deep geological repository. Science of the total environment, 599–600, 348–354.

Cloet, V., M. Pekala, P. Smith, P. Wersin and N. Diomidis. 2017. An Evaluation of Sulphide Fluxes in the Near Field of a HLW Repository. Nagra Report-TR-17-04. Wettingen, Switzerland.

COMSOL, M. v. 5. 6. 2021. Www.comsol.com. COMSOL AB, Stockholm, Sweden, 2021.

Dixon, D., A. Man, S. Rimal, J. Stone and G. Siemens. 2018. Bentonite Seal Properties in Saline Water. Nuclear Waste Management Organization Report NWMO-TR-2018-20. Toronto, Canada.

Dixon, D.A. 2019. Review of the T-H-M-C Properties of MX-80 Bentonite. Nuclear Waste Management Organization Report NWMO-TR-2019-07. Toronto, Canada.

Einstein, A. 1905. Über die von der molekularkinetischen theorie der wärme geforderte bewegung von in ruhenden flüssigkeiten suspendierten teilchen. Annalen der physik, 322, 549–560.

Fick, A. 1855. Ueber diffusion. Annalen der physik, 170, 59–86.

Gascoyne, M. 1997. Evolution of redox conditions and groundwater composition in recharge-discharge environments on the Canadian shield. Hydrogeology Journal, 5, 4–18.

Giroud, N. et al. 2018. On the fate of oxygen in a spent fuel emplacement drift in Opalinus Clay. Applied geochemistry, 97, 270–278.

Gobien, M., F. Garisto, E. Kremer and C. Medri. 2016. Sixth Case Study: Reference Data and Codes. Nuclear Waste Management Organization Report NWMO-TR-2016-10. Toronto, Canada.

Gobien, M., F. Garisto, E. Kremer and C. Medri. 2018. Seventh Case Study: Reference Data and Codes. Nuclear Waste Management Organization Report NWMO-TR-2018-10. Toronto, Canada.

Guo, R. 2016. Thermal Response of a Mark II Conceptual Deep Geological Repository in Crystalline Rock. Nuclear Waste Management Organization Report NWMO-TR-2016-03. Toronto, Canada.

Guo, R. 2018. Thermal Response of a Mark II Conceptual Deep Geological Repository in Sedimentary Rock. Nuclear Waste Management Organization Report NWMO-TR-2018-09. Toronto, Canada.

Hall, D.S., M. Behazin, W. Jeffrey Binns and P.G. Keech. 2021. An evaluation of corrosion processes affecting copper-coated nuclear waste containers in a deep geological repository. Progress in materials science, 118, 1–28.

Hall, D.S., T.E. Standish, M. Behazin and P.G. Keech. 2018. Corrosion of copper-coated used nuclear fuel containers due to oxygen trapped in a Canadian deep geological repository. Corrosion engineering, science and technology, 53, 309–315.

Johansson, A.J. et al. 2020. Corrosion of Copper After 20 years Exposure in the Bentonite Field Tests LOT S2 and A3. Swedish Nuclear Fuel and Waste Management Co Report SKB-TR-20-14. Stockholm, Sweden.

Keech, P.G., M. Behazin, W.J. Binns and S. Briggs. 2021. An update on the copper corrosion program for the long-term management of used nuclear fuel in Canada. Materials and Corrosion, 72, 25–31.

King, F. 2005. Overview of the Corrosion Behaviour of Copper and Steel Used Fuel Containers in a Deep Geologic Repository in the Sedimentary Rock of the Michigan Basin, Ontario. Ontario Power Generation, Nuclear Waste Management Division Report No: 06819-REP-01300-10101-R00. Toronto, Canada.

King, F. 2008. Theory Manual for the Copper Corrosion Model for Uniform Corrosion in Sedimentary Rock CCM-UC.1.1. Nuclear Waste Management Organization Report NWMO TR-2008-07. Toronto, Canada.

King, F. 2009. Microbiologically Influenced Corrosion of Nuclear Waste Containers. Corrosion, 65, 233–251.

King, F., D.S. Hall and P.G. Keech. 2017. Nature of the near-field environment in a deep geological repository and the implications for the corrosion behaviour of the container. Corrosion engineering, science and technology, 52, 25–30.

King, F., M. Kolar and S.S. Gascoyne. 2002. Theory Manual for the Microbiological Copper Corrosion Model CCM-MIC.0. Ontario Power Generation, Nuclear Waste Management Division Report No: 06819-REP-01200-10091-R00. Toronto, Canada.

King, F., M. Kolar and P. Maak. 2008. Reactive-transport model for the prediction of the uniform corrosion behaviour of copper used fuel containers. Journal of nuclear materials, 379, 133–141.

Kremer, E.P. 2017. Durability of the Canadian used fuel container. Corrosion engineering, science and technology, 52, 173–177.

Logan, D.L. 2007. First Course in the Finite Element Method. Thomson Engineering.

Martín, M., J. Cuevas and S. Leguey. 2000. Diffusion of soluble salts under a temperature gradient after the hydration of compacted bentonite. Applied clay science, 17, 55–70.

Millard, A. et al. 2004. Evaluation of THM coupling on the safety assessment of a nuclear fuel waste repository in a homogeneous hard rock. Elsevier Geo-Engineering Book Series, vol. 2, p. 211–216.

Moore, R. 1939. Water conduction from shallow water tables. Hilgardia, 12, 383–426.

Müller, H.R. et al. 2017. Implementation of the full-scale emplacement (FE) experiment at the Mont Terri rock laboratory. Swiss journal of geosciences, 110, 287–306.

Nemes, A., M.G. Schaap, F.J. Leij and J.H.M. Wösten. 2001. Description of the unsaturated soil hydraulic database UNSODA version 2.0. Journal of Hydrology, 251, 151–162.

Nguyen, T.S. and L. Jing. 2005. DECOVALEX III/BENCHPAR PROJECTS Implications of Thermal-Hydro-Mechanical Coupling on the Near-Field Safety of a Nuclear Waste Repository in a Homogeneous Rock Mass. SKI Report 2005:25.

NWMO. 2018. Implementing Adaptive Phased Management 2018 to 2022. Nuclear Waste Management Organization Report. Toronto, Canada.

NWMO. 2019. RD 2019 – NWMO's Program for Research and Development for Long- Term Management of Used Nuclear Fuel. Nuclear Waste Management Organization Report. Toronto, Canada.

Patankar, S.V. 2018. Numerical heat transfer and fluid flow. CRC Press, Boca Raton.

Pedersen, K. 2010. Analysis of copper corrosion in compacted bentonite clay as a function of clay density and growth conditions for sulfate-reducing bacteria. Journal of applied microbiology, 108, 1094–1104.

Rashwan, T.L., M.A. Asad, I.L. Molnar, M. Behazin, P.G. Keech and M.M. Krol. 2022. Exploring the governing transport mechanisms of corrosive agents in a Canadian deep geological repository. Science of The Total Environment, 1–43.

Richards, L.A. 1931. Capillary conduction of liquids through porous mediums. Cornell University,. p. 318–333.

Scully, J.R., D. Féron and H. Hänninen. 2016. Review of the NWMO Copper Corrosion Program. Nuclear Waste Management Organization Report NWMO-TR-2016-11. Toronto, Canada.

Selvadurai, A.P.S. and M. Najari. 2017. The thermo-hydro-mechanical behavior of the argillaceous Cobourg Limestone. Journal of geophysical research: Solid earth, 122, 4157–4171.

Sena, C., J. Salas and D. Arcos. 2010. Thermo-Hydro-Geochemical Modelling of the Bentonite Buffer – LOT A2 Experiment. Swedish Nuclear Fuel and Waste Management Co Report SKB-TR-10-65. Stockholm, Sweden.

Shackelford, C. and S. Moore. 2013. Fickian diffusion of radionuclides for engineered containment barriers: Diffusion coefficients, porosities, And complicating issues. Engineering geology, 152, 133–147.

SKB. 2010. Corrosion Calculations Report for the Safety Assessment SR-Site. Swedish Nuclear Fuel and Waste Management Co Report SKB-TR-10-66. Stockholm, Sweden.

Standish, T. et al. 2016. Corrosion of copper-coated steel high level nuclear waste containers under permanent disposal conditions. Electrochimica acta, 211, 331–342.

Stroes-Gascoyne, S., C.J. Hamon, P. Maak and S. Russell. 2010. The effects of the physical properties of highly compacted smectitic clay (bentonite) on the culturability of indigenous microorganisms. Applied clay science, 47, 155–162.

Sykes, J.F., S.D. Normani and Y. Yin. 2011. Hydrogeologic Modelling. Nuclear Waste Management Organization Report NWMO-TR-2011-16. Toronto, Canada.

Tait, J.C., H. Roman and C.A. Morrison. 2000. Characteristic and Radionuclide Inventories of Used Fuel from OPG Nuclear Generation Stations. Volume 1 –Main report; and Volume 2 – Radionuclide inventory data. Ontario Power Generation, Nuclear Waste Management Division Report No: 06819-REP-01200-10029-R00. Toronto, Canada.

Van Genuchten, M.T. 1980. A closed-form equation for predicting the hydraulic conductivity of unsaturated soils 1. Soil science society of America journal, 44, 892–898.

Villar, M.V., P.L. Martín, I. Bárcena, J.L. García-Siñeriz, R. Gómez-Espina and A. Lloret. 2012. Long-term experimental evidences of saturation of compacted bentonite under repository conditions. Engineering geology, 149–150, 57–69.

Wersin, P. et al. 2014. Sulphide Fluxes and Concentrations in the Spent Nuclear Fuel Repository at Olkiluoto. Posiva Oy Report POSIVA 2014-01. Eurajoki, Finland.